Title	First-Principles Investigations of Cation-Disordered Rock-Salt Type Oxides for Li-Ion Battery Cathodes
Author(s)	濱口, 基之
Citation	大阪大学, 2020, 博士論文
Version Type	VoR
URL	https://doi.org/10.18910/76371
rights	
Note	

First-Principles Investigations of Cation-Disordered Rock-Salt Type Oxides for Li-Ion Battery Cathodes

by

Motoyuki Hamaguchi

Submitted to the Department of Physics, Graduate School of

Science in partial fulfillment of the requirements for the degree of

Doctor of Philosophy in Science

at the

OSAKA UNIVERSITY

March 2020

Supervised by

Dr. Tamio Oguchi

Professor of Institute of Scientific and Industrial Research, Osaka University

First-Principles Investigations of Cation-Disordered Rock-Salt Type Oxides for Li-Ion Battery Cathodes

by

Motoyuki Hamaguchi

Submitted to the Department of Physics, Graduate School of Science
On March 31, 2020, in partial fulfillment of the requirements for the degree of
Doctor of Philosophy in Science

Abstract

The Li-ion battery has achieved a great success as an energy storage system, because of its high capacity, high voltage, and high energy density compared to conventional rechargeable batteries, and is expected to be utilized for future electric vehicles and renewable energy-power grids. Important battery characteristics described above are primarily determined by a cathode material. $3d$-transition metal oxides with well-ordered structures have been considered to be promising candidates for the cathode material. However, their capacities are not enough for large-scale and stationary systems owing to the limited space for Li to incorporate in the crystal, and the structure changes with the O_2-release at low Li concentration cause degrading of the battery performance. In contrast, the oxides of the cation-disordered rock-salt type, in which the cation elements are randomly distributed, are expected to have high structural stability at late charged phases, because Li-vacancy sites are randomly distributed. Furthermore, Li-excess phases with high capacities can be designed by tuning Li concentration in the crystal. Further investigations on these oxides are desirable, because there exist enormous degrees of freedom in the composition of the cation elements which make it difficult to carry out exhaustive experiments.

In the first part of this thesis, $Li_2M TiO_4$ (M = V, Cr, Mn, Fe, Co, and Ni) of the cation-

disordered rock-salt type is studied for the cathode material, and microscopic reaction mechanism including the O_2-release is systematically investigated from first-principles calculation. Electronic structure analyses show that the battery reaction is associated with a mainly M-redox reaction for high Li concentration, whereas that at low Li concentration is associated with an O-redox reaction. Contrary to the speculation, the O_2-release especially at low Li concentration becomes more significant as the number of $3d$ electrons in M is increased. In contrast, the voltage increases as M changes from V to Ni, thus there is a trade-off relation between the voltage and the rechargeable capacity. It is predicted that Li_2CrTiO_4 can be a promising cathode material on owing to the high voltage and high capacity.

In the second part of this thesis, in order to improve the rechargeable capacity, Li-excess phase, $Li_{2+2x}Mn_{1-x}Ti_{1-x}O_4$ ($0 \leq x \leq 0.5$), which does not have rare- and toxic-elements Co and Cr, is theoretically investigated. As predicted in the first part of this thesis, the O-redox reaction with the O_2-release plays significant roles on the battery reaction. Accordingly understanding of the effect of the compositions on the battery characteristics is indispensable to design the cation-disordered cathodes. The structural changes, voltage-capacity profiles, electronic structures, and O_2-release when its chemical compositions x is changed have been theoretically investigated. The Mn- and O-redox reactions play dominant rolls on the compensations for the valence changes by the Li removals, but the O-redox reaction becomes appreciable in the battery reaction at low Li concentrations for high x compositions. Calculated vacancy formation energies of Li and O indicate that the O_2-release from the cathode has sizable contributions to the battery reaction for high x. Finally, it is found that both high rechargeable capacity and high structural stability against the O_2-release are satisfied in $x < 0.2$.

The present results on the effects of transition-metals and Li-excess amounts on the battery performance open a new root to improve the battery performance of cation-disordered rock-salt type oxides for the Li-ion battery.

Thesis Supervisor:
Dr. Tamio Oguchi
Professor of Institute of Scientific and Industrial Research, Osaka University

Acknowledgements

In the begining, I would like to express my sincere gratitude to my supervisor, Professor Tamio Oguchi for the continuous supports in my master and doctoral courses. Your guidance helped me in all the time of my research, and kindly supported my research stays at the university of Groningen in the Kingdom of the Netherlands and the Uppsala university in the Kingdom of Sweden. I could not imagine having invaluable experiences on the visits, and also these experiences helped me to writing of this thesis well. You also allowed me to attend many international and domestic conferences, in which I could have a great experience. Your advices on research as well as on my career have been priceless. You have been a tremendous mentor for me beyond the imagination.

Apart from my Supervisor, I won't forget to express my gratitude to Assistant Professor Hiroyoshi Momida, for his continuous supports. Your advices always guided my research, and also encouraged me in all the time of research. Discussions with you are hard to forget throughout my life.

My sincere thanks also go to Professor Shigeto Okada (Kyushu University) and Associate Professor Ayuko Kitajou (Yamaguchi University), for the invaluable discussions on the Li-ion battery. Your insightful comments from the view point of experiments were helpful for my research.

I would like to also thank my thesis committee members, Professor Kazuhiko Kuroki, Professor Mikito Koshino, and Professor Noriaki Hanasaki, for your brilliant comments and suggestions. Your comments broadened my perspectives, and have made my thesis better.

I am also pleased to say thank you to Associate Professor Koun Shirai, for your valuable advices and for encouraging me as a member of my thesis committee.

I thank my members of Oguchi laboratory for the stimulating discussions and all the fun we have had in the last five years.

Last but not the least, special thanks to my family for supporting me spiritually and financially throughout my master and doctoral courses and my life in general.

Contents

List of Figures

8

List of Tables

Part I

Introduction

1.1 Outlines of the Li-Ion Battery

Batteries are classified into two types; which the ones are disposable (primary) batteries and the others are rechargeable (secondary) batteries. In order to improve the battery performance, many types of primary and secondary batteries have been proposed, and several of them have been commercialized. Leclanché and mercury batteries are typical primary batteries, and lead-acid, nickel-cadmium (Ni-Cd), nickel-hydrogen (Ni-H), and nickel-metal hydride batteries (Ni-MH) are well-known secondary batteries. In two decades, portable electronic devices such as laptop computers and smart phones have been widely used, and the demands for the small size and light weight secondary batteries are increasing. Recently, large-scale energy storage systems for future electric vehicles and renewable energy power grids have become social demands for establishing sustainable society. high voltages, high capacities, and high energy densities are regarded as important factors for evaluations of battery performances, but several additional factors such as costs and environmental impacts must be also considered for designing the systems. The voltage is defined by electric potential differences between a cathode and an anode, indicating that elements with higher standard electrode potential show higher voltages. Therefore, Li element, which is the lightest element and has the highest standard electrode potential, is suitable for the anode material, and rechargeable batteries using Li have been investigated extensively. In 2019, Nobel Prizes in chemistry were given to G. B. Goodenough, M. S. Whittingham, and A. Yoshino for the developments of the Li-ion battery.

The early Li-ion battery developed by Whittingham is composed of a layered rock-salt type $LiTiS_2$ cathode and a pure Li metal anode,[1] and the overall reaction equation of $LiTiS_2$/Li battery is $LiTiS_2 \leftrightarrows TiS_2 + Li$. This $LiTiS_2$/Li battery yields voltage of about 2 V and high capacity exceeding 200 mAh/g.[2] However, the pure Li metal anode shows high reactivity, and Li dendrites upon the Li metal anode, which are generated in charging and discharging reaction processes, have a risk of causing short-circuiting in the battery cell. In order to implement the Li-ion batteries as new secondary batteries with high voltages and high capacities, further studies were required. Important battery characteristics such as the voltage, capacity, and energy

14

density are primarily determined by the cathode material, thus the cathode materials with the battery performances beyond of the $LiTiS_2$ cathode have been explored. A $LiCoO_2$ cathode with the layered rock-salt type structure developed by Goodenough[3] has a maximum capacity of 148 mAh/g and a high average voltage of 3.8 V.[2] This enabled us to use the material as industrial products. After that Goodenough's developments of the $LiCoO_2$ cathode, Yoshino developed improved-graphite anodes,[4] and completed the Li-ion battery with the $LiCoO_2$ cathode and improved-graphite anode. In 1991, the Li-ion battery was first commercialized in Japan around the world, and has been used in a range from a small-size usages for the portable electronic devices to in a large-scale usage for the energy storage systems.

Figure 1.1 shows typical voltages of the representative primary and secondary batteries as a function of capacities. This figure indicates that the Li-ion batteries have higher voltages, higher
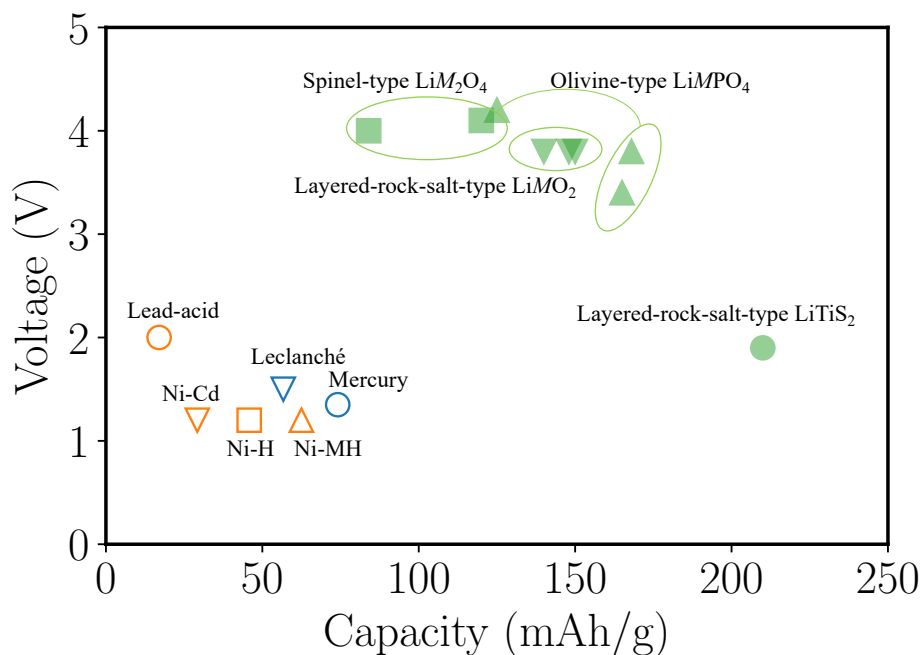
Figure 1.1: Voltages (V) of several primary and conventional secondary, and Li-ion batteries as a function of capacities (mAh/g) are shown in blue marks, orange marks, and green marks. The mercury, Leclanché batteries are plotted by blue circle and blue downward triangle, respectively.[5] The lead-acid (orange blue), Ni-Cd (orange downward triangle), Ni-H (orange square), and Ni-MH (orange upward triangle) batteries are also plotted.[5] The Li-ion batteries are shown separately for each cathode material, which are the layered-rock-salt-type $LiTiS_2$ (green circle) and $LiMO_2$ (green downward triangles), spinel-type LiM_2O_4 (green squares), olivine-type $LiMPO_4$ (green upward triangles).[2]

capacities, and higher energy densities compared to the conventional primary and secondary batteries such as mercury, Leclanché, lead-acid, Ni-Cd, Ni-H, and Ni-MH batteries. The Li-ion battery has potential for use for the electric vehicles and renewable energy power plants in place of traditional automobiles and nuclear power generations. However, drawbacks regarding to safety and costs have been pointed out, and further improvements of the battery performances are required for increasing their potential applications.

1.2 Reaction Mechanisms and Cathode Materials for the Li-Ion Battery

The Li-ion battery is composed of mainly four components, which is a cathode, an anode, an organic electrolyte and a separator. The reaction mechanisms of typical Li-ion battery with $LiCoO_2$ cathode and graphite anode are schematically shown in Fig. 1.2. Typically Li
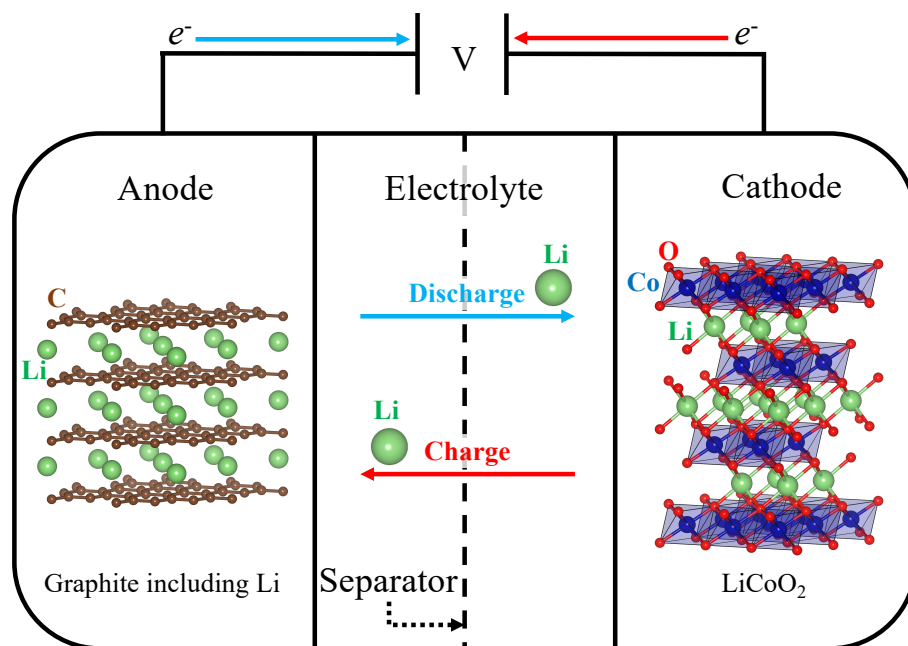
Figure 1.2: Schematic diagram of microscopic reaction mechanisms for the typical Li-ion battery, in which Li-containing graphite and $LiCoO_2$ are utilized as the anode and the cathode material, respectively. The crystal structures of $LiCoO_2$ and graphite including Li are visualized by VESTA.[6]

metal or Li-containing graphite is used for the anode material, whereas several $3d$-transition

metal oxides have been proposed as the cathode material. The organic electrolyte with high ionic conductivities is used because Li has the highest standard electrode potential and thereby reduces most aqueous electrolytes. Therefore, the Li/Li$^+$ potential is utilized for the reference potential in place of the standard hydrogen electrode (SHE). The graphite anode with Li is implemented in the commercialized Li-ion batteries. This does not spoil the voltage because Li in the graphite anode has same chemical potential with the pure Li metal anode. The separator in the electrolyte prevents short-circuiting between the cathode and anode. In the discharge reaction, Li atoms are deintercalated from the anode to the electrolyte, and intercalated from the electrolyte to the cathode. In contrast, Li atoms are deintercalated from the cathode to the electrolyte, and intercalated from the electrolyte to the anode in the charge reaction. The schemes of the reactions are the same among different electrode materials.

Hence, reaction mechanisms are explained by the case of the LiCoO$_2$ cathode and the Li-metal anode as a representative example. Half reaction equations of the LiCoO$_2$/graphite battery are written by

$$\text{Anode} \quad : \quad \text{Li}_x\text{C} \rightleftarrows \text{C} + x\text{Li}^+ + xe^-, \tag{1.1}$$

$$\text{Cathode} \quad : \quad \text{CoO}_2 + x\text{Li}^+ + xe^- \rightleftarrows \text{Li}_x\text{CoO}_2. \tag{1.2}$$
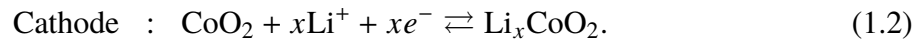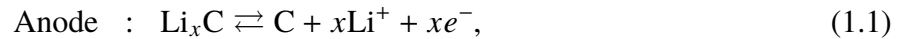
The theoretical capacity C of this Li-ion reaction is calculated, using a molecular weight 98 of LiCoO$_2$ and the Faraday constant $F = 9.65 \times 10^4$ C/mol, by

$$C = \frac{9.65 \times 10^4 \times 1000}{60 \times 60 \times 98} = 274\text{mAh/g}, \tag{1.3}$$

on the assumption that, in reaction Eq. (1.2), 1 mol of electrons is emitted/absorbed for a unit reaction of 1 mol of LiCoO$_2$.

The voltages can be theoretically estimated by SHEs of Li and reaction elements. In the LiFePO$_4$ cathode, Fe^{2+}/Fe^{3+} reduction- and oxidation- (redox) reactions are considered in the

17

stoichiometric reaction equation written by

$$Li^+Fe^{2+}PO_4^{3-} \rightleftarrows Fe^{3+}PO_4^{3-} + Li. \tag{1.4}$$
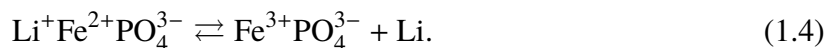
The Fe^{2+}/Fe^{3+} redox potential against SHE is 0.771 V, and the Li/Li^+-redox potential against SHE is evaluated as -3.040 V.[7] Hence, the average voltage is estimated as 3.811 V. Note that, as to be precise, the Fe^{2+}/Fe^{3+}-redox potential in the $LiFePO_4$ cathode is not necessarily same as that in aqueous solvents. And it is possible that the Fe^{2+}/Fe^{3+}-redox mechanism assumed by the ionic representations is different with the real bulk systems.

As described previously, the essential battery characteristics, for example the voltage, capacity, and energy density, are primarily determined by the cathode material, thus many cathode materials have been investigated extensively, especially in $3d$-transition metal oxides.[2, 8–10] In order to further improve the battery performance and to lower material costs, several types of the cathode materials have been reported experimentally, for example, $LiCoO_2$ with the layered rock-salt-type structure,[3] $LiMn_2O_4$ with the spinel-type structure,[11] and $LiFePO_4$ with the olivine-type structure[12], shown in Fig. 1.3. For these cathode materials, structural, electrochem-

(a) Layered-rock-salt-type LiCoO₂   (b) Spinel-type LiMn₂O₄   (c) Olivine-type LiFePO₄
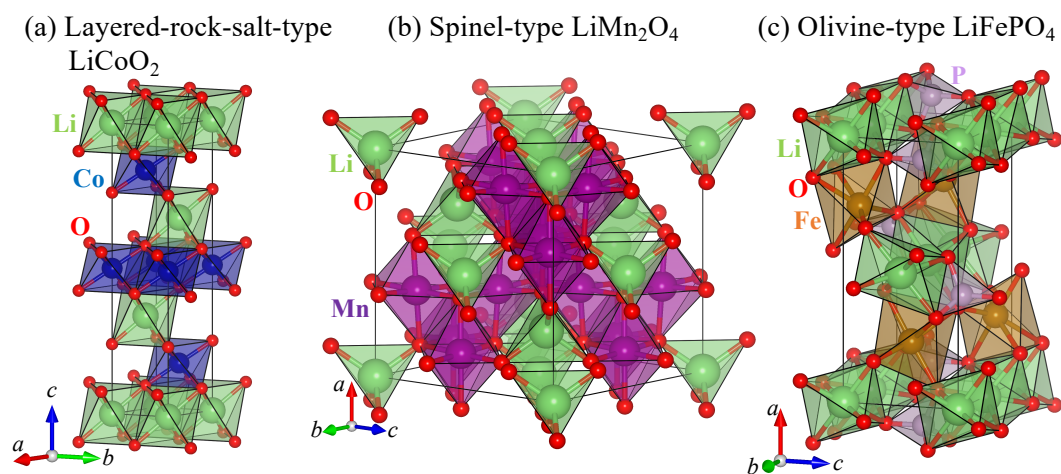
Figure 1.3: (a) layered-rock-salt-type $LiCoO_2$, (b) spinel-type $LiMn_2O_4$, and (c) olivine-type $LiFePO_4$ visualized by VESTA.[6]

ical, and electronic properties have been investigated using first-principles calculations.[13–15] Crystal structures, theoretical and experimental capacities, average voltages, and phase stages in development for the cathode materials with the layered-rock-salt-, spinel-, and olivine-type

structures and those of Li_2MTiO_4 with the cation-disordered rock-salt type structure are listed in Table 1.1. The layered rock-salt type $LiTiS_2$ is the first developed cathode material in the

Table 1.1: Crystal structures, theoretical and experimental capacities, average voltages, and phase stages in development for typical cathode materials with the layered-rock-salt-, spinel-, and olivine-type structures are listed.[2] Those of Li_2MTiO_4 with the cation-disordered-rock-salt type structure are also listed for M = V,[35] Cr, Mn,[40,41] Fe,[33] Co,[36] and Ni.[32,33,37,38]

Crystal structure	Compound	Capacity (mAh/g) (Theo./ Exp.)	Average voltage (V)	Phase stage in development
Layered rock-salt	$LiTiS_2$	225/210	1.9	Commercialized
	$LiCoO_2$	274/148	3.8	Commercialized
	$LiNiO_2$	275/150	3.8	Research
	$LiMnO_2$	285/140	3.3	Research
Spinel	$LiMn_2O_4$	148/120	4.1	Commercialized
	$LiCo_2O_4$	142/84	4.0	Research
Olivine	$LiFePO_4$	170/165	3.4	Commercialized
	$LiMnPO_4$	171/168	3.8	Research
	$LiCoPO_4$	167/125	4.2	Research
Cation-disordered rock-salt	Li_2VTiO_4	303/165	3.3	Research
	Li_2CrTiO_4	301.6/None	None	Not synthesized
	Li_2MnTiO_4	297/112-145	3.15-3.375	Research
	Li_2FeTiO_4	295/18	2.925	Research
	Li_2CoTiO_4	290/144.3	3.15	Research
	Li_2NiTiO_4	291/96-182	3.375-3.85	Research

world by Nobel winner M.S. Whittingham, but its average voltage is not so high compered to other cathode materials. The $LiCoO_2$ with layered rock-salt-type structure is commercially the most successful cathode material, showing a high average voltage of 3.8 V and a high theoretical capacity of 274 mAh/g.[2] The $LiCoO_2$ structure is composed of the Li layer and the CoO_6-octahedra layer in a manner of alternate structures, and Li ions can diffuse in the *ab* plane. However, the $LiCoO_2$ cathode has serious problems regarding to safety and costs. The safety problem is that structure deformations can occur when more than 50 % of Li atoms in the $LiCoO_2$ cathode are desorbed from the cathode during the charge reaction process. The deformation induces degradations of the capacity and the O_2-release from the cathode material. Available rechargeable capacity is limited by only half of the theoretical one because the desorbed O_2 gas exothermically reacts with the organic electrolyte.[16–18] The problem of costs is

due to the fact that $LiCoO_2$ includes rare- and toxic element Co. The $LiFePO_4$ with the olivine type structure has FeO_6 octahedra and PO_4 tetrahedra, which share their vertexes each other, showing the stable crystal structures after Li dissociation, and Li-atoms can diffuse along to the b-axis. $LiFePO_4$ is an excellent superior cathode material on owing to the low costs and low environmental impacts, but its theoretical capacity of 170 mAh/g is not so large. Similarly, the $LiMn_2O_4$ with the spinel type structure shows small theoretical capacity of 148 mAh/g. Recently, the layered rock-salt type $LiNi_xCo_{1-2x}Mn_xO_2$, which can be obtained by partially replacing Co in $LiCoO_2$ with Ni and Mn, has been reported as an alternative cathode material, showing high thermodynamical stability.[19, 20] However, Li^+ and Ni^{2+}, which have nearly same ionic radii, are mixed in the oxide, and Ni atoms inserted in the Li layer prevent Li from diffusion during the battery reaction.[19, 20]

The cathode properties of the commercialized or nearly-commercialized cathode materials were described above, but cathode materials showing other reaction mechanisms also have been proposed for the Li-ion battery. The cathode materials are generally divided into two types according to the reaction mechanisms; the ones are intercalation-type cathode materials and the others are conversion-type cathode materials. Materials with the layered-rock-salt-, spinel-, and olivine-type structures belong to the intercalation-type cathode materials, and many of them have been commercially succeeded. In the intercalation-type cathode materials, the backbone of the CoO_6-octahedra layers is untouched upon Li-insertion and desorption, resulting in the high cycle performances (cyclabilities) of this type. On the other hand, in the conversion-type cathode materials, there is no steady structure, and the crystal structures drastically change during the reaction processes. This-type cathode material has high theoretical capacity, because it does not need open spaces for accommodation of Li, but their cyclabilities are generally lower than those of the intercalation-type cathode materials because of the drastic structural changes during the charge and discharge reactions.

1.3 First-Principles Approaches to Study the Li-Ion Battery

Developments of the Li-ion batteries historically have been proceeded by electrochemical experiments, whereas systematic experimental investigations on the basis of element-selective analyses become much difficult because the cathode materials studied recently include many different kinds of elements and large material spaces. First-principles calculations can calculate important physical quantities without empirical and experimental parameters, and electronic structures can be obtained each element, *i.e.*, the first-principles calculation is regarded as the simulation technique with both element-selective- and parameter-free-analyses.

The first-principles calculation is known as a band calculation in the field of solid-state physics, because this technique calculates electronic (band) structures of materials. To strictly calculate electronic structures of materials on the basis of quantum mechanics, Schrödinger equations for many-body systems are needed to be calculated. However, it is impossible to calculate Schrödinger equations for many-body systems. The theoretical system that makes it possible to calculate wave functions for the many-body system is the density functional theory (DFT) composed of the Hohenberg-Kohn's theorem,[21] and nowadays the first-principles calculation generally means the calculation technique on the basis of the DFT. The first-principles calculation scheme is composed of mainly following three steps.

1. An interacting many-electron problem is mapped onto a non-interacting many-electron problem, by using the DFT, which is known as one-electron approximation because a non-interacting many-electron problem can be replaced to a one-electron problem.

2. The one-electron equation (Kohn-Sham equation) is self-consistently calculated, giving electron densities.

3. Various physical quantities of materials such as total energies can be calculated using the electron densities.

In order to investigate the reaction mechanism of the cathode materials during the battery reactions, the first-principles calculation is performed for structure models corresponding to each

Li concentration from fully discharged (lithiated) phase to fully charged (delithiated) phase. In the intercalation-type cathode materials, the crystal structures of the reaction intermediates are experimentally observed by X-ray diffraction (XRD) measurements. Structure models corresponding to each Li concentration are generated by removing Li from the pristine models, because the host structures are kept during the charge and discharge reaction processes. In the conversion-type cathode materials, the crystal structures of the intermediates are not often revealed experimentally, but the reaction mechanisms can be investigated according to predicted structure models, which are explored by crystal structure prediction algorithms. The crystal structure prediction algorithms predict the stable crystal structures with given chemical compositions among several crystal structures on the basis of the calculated total energies. The first-principles calculation can calculate the total energy by minimal input data such as atomic numbers without the empirical and experimental parameters, consequently, the crystal structures of the reaction intermediates, which have no experimental data, can be predicted by using the crystal structure prediction algorithms. There exist enormous degrees of freedom as to which elements are located where in the cell, even if the chemical compositions are given. Hence, many fast-exploration techniques such as the evolutionary algorithm and Bayesian optimization have been proposed for this problem. USPEX[22–24] and CrySPY[25,26] are known as the typical crystal structure prediction algorithms. Li- and Na- ions are (de-)intercalated in the cathodes and the anodes for the Li- and Na-ion batteries, thus chemical compositions except for Li or Na composed of the electrodes are generally fixed during the charge and discharge reaction processes. Therefore, theoretical studies have been performed using the crystal structure prediction algorithms for $Na_xC_6O_6$[27] and SnS[28,29] of the cathode and anode materials, respectively.

The voltage-capacity profile of the $LiCoO_2$ cathode is studied as an example of investigations for the cathode properties on the basis of the first-principles calculation.[13] The average voltage is defined by the electric potential difference between the cathode and anode, and the Li/Li^+-redox potential is practically adopted for the reference electrode potential in both the Li-metal anode and other anodes such as the graphite anode. Therefore, the average voltage is calculated

22

against the Li-metal anode. The half reaction equations are written by

$$\text{Anode} \quad : \quad (x_2 - x_1)\text{Li} \rightleftarrows (x_2 - x_1)\text{Li}^+ + (x_2 - x_1)e^-, \tag{1.5}$$

$$\text{Cathode} \quad : \quad \text{Li}_{x_2-x_1}\text{CoO}_2 + (x_2 - x_1)\text{Li}^+ + (x_2 - x_1)e^- \rightleftarrows \text{Li}_{x_2}\text{CoO}_2. \tag{1.6}$$
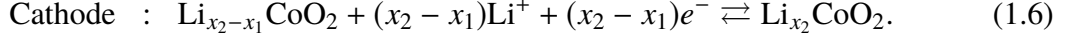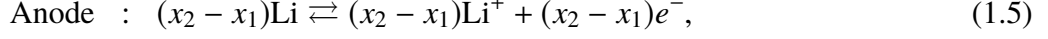
, where x_1 and x_2 are satisfied with $x_2 \geq x_1$. The open-circuit average-voltage V (V = J/C) of the Li-ion battery is defined using the chemical potential of Li μ_{Li} (J/mol) differences between in the cathode and in the anode by

$$V(x) = -\frac{\mu_{\text{Li}}^{\text{cathode}} - \mu_{\text{Li}}^{\text{anode}}}{zF} \tag{1.7}$$

, where F is the Faraday constant (C/mol) and z is the number of electrons transferred in the electrolyte. If all charge transfer in the electrolyte is associated with Li$^+$ transfer, $z = 1$ is satisfied, because Li is intercalated to the electrode as Li$^+$. In Eq. (1.7), each physical quantity per one mol is considered, but it is mapped onto per one atom, or electron-volt unit hereinafter to establish consistency with the calculation results of the first-principles calculation. The Faraday constant F equals to the elementary charge e in electron-volt unit, because the Faraday constant is defined by electric charges per one mol of electrons. Eq. (1.7) can be written by

$$V(x) = -\frac{\mu_{\text{Li}}^{\text{cathode}} - \mu_{\text{Li}}^{\text{anode}}}{e}. \tag{1.8}$$

The chemical potential of Li in the cathode increases with increasing Li concentration in the cathode, and the average voltage V decreases during the discharge reaction process. Electrical work W (eV) associated with the discharge from $\text{Li}_{x_1}\text{CoO}_2$ to $\text{Li}_{x_2}\text{CoO}_2$ is obtained by an integration from 0 to $q_{\text{tot}} = (x_2 - x_1)e$ of the product between the average voltage $V(x)$ (V) and electric charge displacements dq (C), *i.e.*

$$W = \int_0^{q_{\text{tot}}} V(x)dq = -\int_0^{q_{\text{tot}}} \frac{\mu_{\text{Li}}^{\text{IC}} - \mu_{\text{Li}}^0}{e} \tag{1.9}$$

, where $\mu_{\text{Li}}^{\text{IC}}$ and μ_{Li}^{0} are the chemical potentials of Li in the cathode and Li-metal anode, respectively. The chemical potential of Li in the Li-metal anode equals to the Gibbs free energy of metal Li and is independent of x. The chemical potential of Li in the cathode also equals to the Gibbs free energy in the one-particle (electron-volt unit) representation. Assuming that the change of electric charge is associated with Li transfer, using $dq = edx$, the electrical work W is written by

$$
\begin{aligned}
W &= -\int_{x_1}^{x_2} \left\{ \mu_{\text{Li}}^{\text{IC}}(x) - \mu_{\text{Li}}^{0} \right\} dx \\
&= -\left\{ G_{\text{Li}_{x_2}\text{CoO}_2} - G_{\text{Li}_{x_1}\text{CoO}_2} - (x_2 - x_1)G_{\text{Li}} \right\} \\
&= -\Delta G_r
\end{aligned}
\tag{1.10}
$$

Therefore, using electrical work W, which is needed to transfer $(x_2 - x_1)$ electrons, the average voltage $\overline{V}$ during the discharge reaction process from $\text{Li}_{x_1}\text{CoO}_2$ to $\text{Li}_{x_2}\text{CoO}_2$ in the LiCoO_2 cathode is written by

$$
\overline{V} = \frac{W}{x_2 - x_1} = \frac{-\Delta G_r}{x_2 - x_1}.
\tag{1.11}
$$

Assuming that the calculated cathode system have nearly equilibrium volume at the range of low temperatures, $\Delta G_r \simeq \Delta E_r$ is approximately valid, because the displacement terms of volume $(P\Delta V_r)$ and entropy $(T\Delta S_r)$ in $\Delta G_r (\equiv \Delta E_r + P\Delta V_r - T\Delta S_r)$ are enough small to be negligible. This approximation is considered to be reasonable, because the term $|P\Delta V_r|$ is of the order of about 10^{-5} eV and $|T\Delta S_r| \ll |\Delta E_r|$ is valid, while the term $|\Delta E_r|$ per one molecular is of the order of a few eV.[13] Assuming this approximation, the average voltage $\overline{V}$ in Eq. (1.11) can be written by, using the changes of the internal energy (ΔE_r),

$$
\overline{V} = \frac{-\Delta E_r}{x_2 - x_1} = -\frac{E(\text{Li}_{x_2}\text{CoO}_2) - E(\text{Li}_{x_1}\text{CoO}_2) - (x_2 - x_1)E(\text{Li})}{x_2 - x_1}
\tag{1.12}
$$

, where $E(X)$ is the total-internal energy of the material X, showing that the average voltage

$\overline{V}$ can be evaluated using the calculated total energies of the reaction intermediates and pure Li metal. As discussed previously, removing all Li from the $LiCoO_2$ cathode with the layered rock-salt type structure is difficult, because the structure deformations take place at low Li concentration in the cathode. If the fully-lithiated $LiCoO_2$ phase and delithiated (CoO_2) phase are assumed as the pristine and the end point of the battery reaction as the most simplified example, the half reaction equation in the cathode can be written by

$$LiCoO_2 \rightleftarrows CoO_2 + Li^+ + e^-. \tag{1.13}$$

Using $x_2 = 1$ and $x_1 = 0$, Eq. (1.12) is given by

$$\overline{V} = -\left\{ E(LiCoO_2) - E(CoO_2) - E(Li) \right\}, \tag{1.14}$$

The calculated average voltage of 3.71 V, which is in good agreements with experimental value of 3.8 V,[2] is obtained by performing the first-principles calculation for $LiCoO_2$, CoO_2, and pure Li metal. Similarly, this investigation scheme can be adopted for the conversion-type cathode FeS_2 for the Na-ion battery, and its predicted average voltage also reproduces experiments.[30]

1.4 Cation-Disordered Rock-Salt Oxides for Li-Ion Battery Cathodes

Although many cathode materials especially $3d$-transition metal oxides have been investigated both experimentally and theoretically,[2, 8–10] only the intercalation-type cathode materials with the cation-ordered structures were considered to have suitable characteristics for the commercial use in terms of the voltages, capacities, and cycle performances. The diffusivity of Li atoms in the cation-ordered structures is expected to be large, because other cations such as heavy $3d$-transition metals do not disturb the diffusion of Li atoms, suggesting the good cycle performances and rate characteristics. However, the amounts of removable Li, which determine

the rechargeable capacities, depends on the open spaces for Li in the parent phases, thus it is difficult to dope Li atoms excessively in transition-metal oxides with well-ordered structures to improve the rechargeable capacities. Furthermore, the cathode materials with the cation-ordered structures especially the layered-rock-salt-type structure exhibit the structure deformations at low Li concentration.[16–18] Even if the structure deformations can be suppressed by partially replacing Co with Mn and Ni, cation mixing between Li^+ and Ni^{2+} leads to impede the diffusion of Li atoms.[19, 20] To increase the rechargeable capacities and to the improve structural stability, different strategies for designing the new cathode materials are desired.

Recently, the cation-disordered rock-salt type Li_2MTiO_4 (M = V, Mn, Fe, Co, and Ni),[31–41] $Li_{1.211}Mo_{0.467}Cr_{0.3}O_2$,[42] $Li_{1.2}Ni_{1/3}Ti_{1/3}Mo_{2/15}O_2$,[43] and $Li_{1.15}Ni_{0.45}Ti_{0.3}Mo_{0.1}O_{1.85}F_{0.15}$[44] have been proposed as the cathode materials for the Li-ion batteries. These cathode materials do not have layered structures, as found in $LiCoO_2$ and $LiNi_xCo_{1-2x}Mn_xO_2$, but have rock-salt (face-centered cubic: FCC) type structures with space group $Fm\bar{3}m$. The structure is shown in Fig. 1.4. The cation elements including Li are randomly distributed on the FCC sub-lattice.
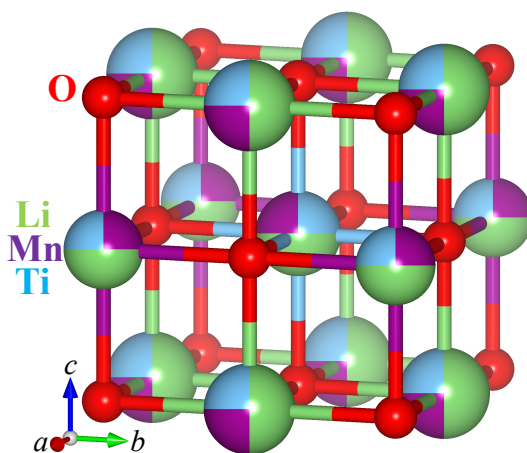
Figure 1.4: Crystal structure of Li_2MnTiO_4 with cation-disordered rock-salt type structure. Green, purple, blue, and red spheres show Li, Mn, Ti, and O, respectively. This figure is rendered by VESTA.[6]

Consequently, vacancies of Li atoms are also randomly distributed, and the crystal structure is expected to maintain during the battery reaction, resulting in the high-structural stability at low Li concentration. Furthermore, there exist enormous degrees of freedom in the compositions of cation elements, which can be tuned well, thus these oxides of the cation-disordered rock-

salt type have good candidates as the cathode materials compared to the layered-rock-salt-type cathodes. Although the oxides of the cation-disordered rock-salt type are promising candidates for the cathode materials, low diffusivity of Li is an unavoidable problem for these oxides. In 2014, Ceder and co-workers proposed oxides of the Li-excess cation-disordered rock-salt type as the cathode materials for the Li-ion batteries. They indicated that the diffusivity of Li atoms is remarkably improved by increasing Li concentration in the oxides.[42] The cation-disordered rock-salt type oxides and their Li-excess phases have been investigated theoretically and experimentally again.

1.5   Purpose

The cation-disordered rock-salt type oxides are promising cathode materials, because the oxides have advantages regarding to the high capacities and high structural stability compared to the conventional oxides. These oxides include many different chemical species for the cation, thus their reaction mechanisms are complex compared to the simple Co^{3+}/Co^{4+}-redox reaction in the $LiCoO_2$ cathode. There are enormous degrees of freedom in the chemical composition, thus the systematic and element-selective investigations for these oxides are experimentally difficult. To clarify the reaction mechanisms and to optimize the chemical compositions of these oxides are required for improving the Li-ion batteries. However, the first-principles calculation, which is the element-selective and the parameter-free analysis technique, have not sufficiently examined for these oxides. In this study, the cathode materials of the cation-disordered rock-salt type are studied using the first-principles calculations. The microscopic reaction mechanisms depend on the chemical composition are systematically investigated on the basis of the calculated electronic structure changes associated with Li insertion an desorption.

1.6   Overview of this thesis

The cation-disordered rock-salt type oxides are investigated as the cathode materials for the Li-ion batteries using the first-principles calculations, and new chemical compositions and Li-excess phases with the good cathode performances are proposed in this thesis.

In the first part of this thesis, the cathode properties of the cation-disordered rock-salt type $Li_2M TiO_4$ (M = V, Cr, Mn, Fe, Co, and Ni) are theoretically studied from the aspect of the O_2-release during the charge and discharge reaction processes. The reason why experimental rechargeable capacities are smaller than the theoretical ones is clarified by analyzing the O_2-release and anion (O)-redox reaction. The O-redox reaction in addition to conventional cation (metal)-redox reactions enhance the capacities, but the present calculated electronic structures show that the electronic states are unstable because of doping holes in O-$2p$ states. The voltage increases as M changes from V to Ni, but the tend of the low structural stability is enhanced with increasing number of $3d$ electrons in M. Therefore, it is concluded that Li_2CrTiO_4 may be the best candidate for the cathode material satisfied with both high voltage and high structural stability among the oxides.

In the second part of this thesis, the chemical composition of Li is optimized for the Li-excess cation-disordered rock-salt type $Li_{2+2x}Mn_{1-x}Ti_{1-x}O_4$ without the rare and toxic element. The effect of Li-excess x on the battery characteristics is investigated theoretically, and the Li-excess x is optimized for the capacities and structural stability against the O_2-release from the cathodes. The battery reaction is predominantly determined by Mn- and O-redox reactions, and the O-redox reaction becomes more important, because the oxidation of Mn is limited by Mn^{4+} as x increases. Furthermore, the contribution of the O_2-release from the cathode on the battery reaction cannot be negligible for high x phases, suggesting that $x < 0.2$ is suitable for the cathode materials, because of the high structural stability against O_2-release during the charge and discharge reaction processes.

Part II

Cathode Properties of Li$_2$*M*TiO$_4$

(*M* = V, Cr, Mn, Fe, Co, and Ni)

with O$_2$-Release for the Li-Ion Battery

3.1 Introduction

As described in Part I, $LiCoO_2$ with the layered rock-salt type structure has drawbacks for safety and costs. The oxides of cation-disordered rock-salt type are the promising cathode materials as substitutes for the well-ordered oxides. In the $LiCoO_2$ cathode, the O_2-release, which is resulted in the structure deformations originating from the unstable structures at low Li concentration, causes a serious problem for safety because the dissociated O_2 exothermically reacts with the organic electrolyte.[16–18] Furthermore, the $LiCoO_2$ cathode is highly expensive and has high-environmental impacts because Co is one of the rare and toxic elements. A series of lithium transition-metal titanates Li_2MTiO_4 (M = V, Mn, Fe, Co, and Ni) with the cation-disordered rock-salt type structure have been studied experimentally,[31–41] since the first synthesis and oxidative Li-dissociation of the oxides were reported in 2003,[31] relatively earlier compared to other cathode materials of the cation-disordered rock-salt type.[42–44] No electrochemical measurement for the battery characteristics of these oxides in the Ref[31] was performed. Soon their battery characteristics, with M = V newly added, were electrochemically investigated in after 2004.[32–41] Li_2MTiO_4 is the oxide with the typical cation-disordered rock-salt type structure with space group $Fm\overline{3}m$, and cation elements of Li, M, and Ti are randomly distributed on the FCC sub-lattice. Each cation element is located on the center of octahedral unit with six nearest neighbor O atoms, and the MO_6 octahedra share their edges each other, forming a densely closed-packed crystal structure compared to oxides with large open spaces for Li. Therefore, the O_2-release from the cathode is expected to be strongly suppressed during the charge and discharge reaction processes, and it is also predicted that group 4 element; Ti as Ti^{4+} strongly attracts O and enhances the structural stability.[41]

The stoichiometric reaction equation of an overall cell for the Li_2MTiO_4 cathode with the metal Li anode is written as

$$Li_2MTiO_4 \rightleftarrows MTiO_4 + 2Li, \tag{3.15}$$

and the battery reaction mechanism is stoichiometrically associated with M^{2+}/M^{3+}- and

M^{3+}/M^{4+}-redox reactions for $0 \leq y \leq 1$ and $1 \leq y \leq 2$, respectively, in the Li concentration $(2 - y)$, on the assumption of the rigid-ion model: Li^+, Ti^{4+}, and O^{2-}. Assuming that the two-electron reaction, namely the M^{2+}/M^{4+}-redox reaction, can occur with the Eq. (3.15), the theoretical capacities of 303.4, 301.6, 296.6, 295.2, 290.2, and 290.6 mAh/g are calculated for M = V, Cr, Mn, Fe, Co, and Ni, respectively, which are roughly twice as large as the experimental rechargeable capacity of the LiCoO$_2$ cathode. However, their measured rechargeable capacities are different from the predicted ones, suggesting that the above reaction mechanism is wrong. The experimental rechargeable capacities at room temperatures are only 165 mAh/g for Li$_2$VTiO$_4$,[35] 112-145 mAh/g for Li$_2$MnTiO$_4$,[40, 41] 18 mAh/g for Li$_2$FeTiO$_4$,[33] 144 mAh/g for Li$_2$CoTiO$_4$,[36] and 96-182 mAh/g for Li$_2$NiTiO$_4$,[32, 33, 37, 38] corresponding to the theoretical capacities for one-electron reactions, and suggesting that different or additional reactions to the stoichiometric reaction may occur during the charge and discharge reaction processes. The previous experiments indicated that the Ti- and O-redox reactions contribute to the battery reaction, suggesting that the complex redox reaction associated with multiple elements occur in the cathodes. Kitajou et al. reported for Li$_2$MnTiO$_4$ by in-situ X-ray absorption near-edge structure (XANES) measurements that the reaction has two steps; the first step is the Mn^{2+}/Mn^{3+}- redox reaction at high Li concentrations, and the second one is the $O^{2-}/(O_2)^{2-}$-redox reaction at low Li concentrations in the cathode.[41] Similarly, Yang et al. have performed electrochemical experiments for Li$_2$CoTiO$_4$, indicating Co^{2+}/Co^{4+}- and Ti^{3+}/Ti^{4+}-redox couples.[36] Kawano et al. reported for Li$_2$NiTiO$_4$ that Ni^{2+}/Ni^{3+}- and Ti^{3+}/Ti^{4+}-redox couples contribute to the battery reaction.[38] In addition, contrary to the expectation for the suppressing O$_2$-release from the cathode, Prabaharan et al. and Trócoli et al. showed the O$_2$-release from the cathode in Li$_2$NiTiO$_4$.[32, 37]

As described above, several different microscopic reaction mechanisms depending on M have been proposed by the previous experimental studies, and coherent understanding is lacked for improving and designing the future cathode materials with the cation-disordered rock-salt type structures. In addition, the effects of the O$_2$-release and O-redox reaction on the battery reaction have been investigated intensively in other cathode oxides.[45–47] Therefore, a systematic

31

study for the oxides is needed.

In the first part, the cathode properties of Li_2MTiO_4 (M = V, Cr, Mn, Fe, Co, and Ni) are theoretically studied by a first-principles calculation. The cycle characteristics are discussed on the basis of the calculated structure changes with Li insertion and desorption, and formation enthalpies of $Li_{2-y}MTiO_4$ with several Li concentration ($2 - y$) are calculated to obtain the theoretical reaction passes, which are used for calculations of voltage-capacity characteristics. The calculated voltage-capacity characteristics are discussed by comparison with experimental results, and the redox reaction in each reaction stage is investigated on the basis of calculated electronic structure changes associated with the Li insertion and desorption. Second, the O_2-release from the cathode is focused. Li- and O-vacancy formation energies are calculated to theoretically evaluate the structural stability against the O_2-release during the charge and discharge reaction processes. Finally, on the basis of the findings about the microscopic reaction mechanism including the O_2-release for all M, the best potential oxide for the cathode use among the calculated materials in terms of the voltages, capacities, and structure stability against O_2-release is discussed and proposed.

3.2   Models and Method

Calculated model structures of $Li_{2-y}MTiO_4$ (M = V, Cr, Mn, Fe, Co, and Ni) for y = 0, 0.5, 1, 1.5, and 2 with rock-salt-based structures, shown in Fig. 3.1. The smallest and simplest supercell is used in order to model $Li_{2-y}MTiO_4$ with the cation-disordered rock-salt type structure, because d^0-transition metals can tolerate displacements and configurations of cation sites with relatively small energy differences, consequently, the effect of the cation-site configurations and the Jahn-Teller distortions are considered to be negligible.[48] Figure 3.1 (a) shows the basic model with space group *P4/mmm* for y = 0 including one formula unit (eight atoms) in the cell, and Fig. 3.1 (b) and 3.1 (c) show the models with space group *Pmmm* and *P4/mmm* for y = 1 and 2, which are prepared by removing one and two Li atoms from the model for y = 0, respectively. The models with space group *Cmmm* for y = 0.5 and 1.5 are generated as
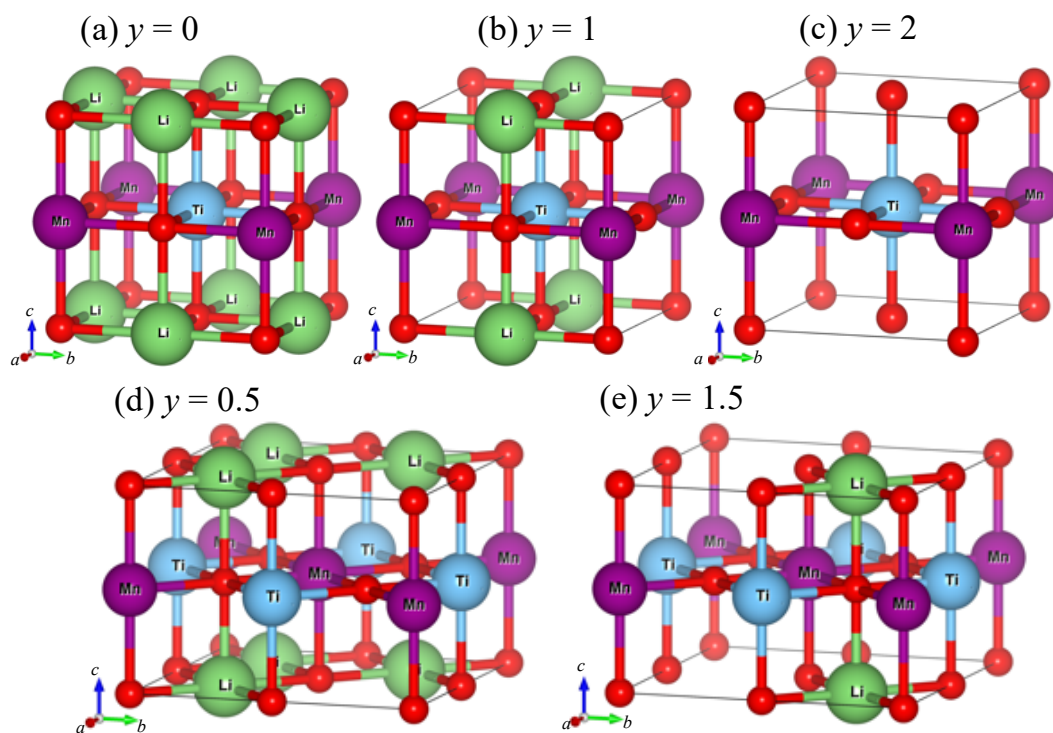
Figure 3.1: Model structures of $Li_{2-y}M\mathrm{TiO_4}$ (M = V, Cr, Mn, Fe, Co, and Ni) for y = 0, 0.5, 1, 1.5, and 2: (a) $Li_2M\mathrm{TiO_4}$ (y = 0), (b) $LiM\mathrm{TiO_4}$ (y = 1), (c) $M\mathrm{TiO_4}$ (y = 2), (d) $Li_{1.5}M\mathrm{TiO_4}$ (y = 0.5), (e) $Li_{0.5}M\mathrm{TiO_4}$ (y = 1.5). Green, purple, blue, and red spheres show Li, M, Ti, and O, respectively. These figures were visualized by VESTA.[6]

$\sqrt{2} \times \sqrt{2} \times 1$ supercells of the model for $y = 0$ by removing Li atoms, thus these models include

sixteen atoms in conventional cells, shown in Fig. 3.1(d) and (e), respectively. Table 3.1 lists

the detailed information of the model structure for $Li_{2-y}MTiO_4$. To evaluate the O_2-release

Table 3.1: Space groups and Wyckoff positions of the calculated model structure of $Li_{2-y}MTiO_4$ (M = V, Cr, Mn, Fe, Co, and Ni) for y = 0, 0.5, 1, 1.5, and 2.

y	0	0.5	1	1.5	2
Model (Space group)	Li_2MTiO_4 (*P4/mmm*)	$Li_3M_2Ti_2O_8$ (*Cmmm*)	$LiMTiO_4$ (*Pmmm*)	$LiM_2Ti_2O_8$ (*Cmmm*)	$MTiO_4$ (*P4/mmm*)
Wyckoff sites	Li1 $2f$	Li1 $4f$	Li1 $1e$	Li1 $2d$	M1 $1b$
	M1 $1b$	Li2 $2c$	M1 $1c$	M1 $4g$	Ti1 $1d$
	Ti1 $1d$	M1 $4g$	Ti1 $1h$	Ti1 $4i$	O1 $1a$
	O1 $1a$	Ti1 $4i$	O1 $1a$	O1 $4h$	O2 $1c$
	O2 $1c$	O1 $4h$	O2 $1f$	O2 $4j$	O3 $2e$
	O3 $2e$	O2 $4j$	O3 $1g$	O3 $2a$	
		O3 $2a$	O4 $1d$	O4 $4e$	
		O4 $4e$		O5 $2b$	
		O5 $2b$			

from Li_2MTiO_4, the x = 0, 1, and 2 models shown in Fig. 3.1(a)- 3.1(c), respectively, are used,

and some O atoms are removed from the cells by finding vacancy sites with the lowest energies.

First-principles calculation is performed with the local density approximation (LDA),[49] and

the Kohn-Sham equation is solved self-consistently by using all-electron scaler-relativistic full-

potential linearized augmented plane wave (FLAPW) method.[50–54] Computations are carried

out using the HiLAPW code,[55] which has been successfully adopted for several electrode

materials such as $Na_xC_6O_6$, SnS, and $NaFeSO_4F$ for the Na-ion batteries.[27–30, 56–60] Muffin-tin

radii of 0.8 Å for Li and O, 0.9 Å for Ti, 1.1 Å for V, and 1.0 Å for Cr, Mn, Fe, Co, and Ni are

used, and cut-off energies of 20 Ry and 160 Ry are adopted for the wave function and potential

basis sets, respectively. The $\boldsymbol{k}$-space integrations are carried out using the improved tetrahedron

method,[61] and the structure optimizations are treated with uniform $\boldsymbol{k}$-meshes of $8 \times 8 \times 8$ for

the y = 0, 1, and 2 models and $3 \times 3 \times 6$ for the y = 0.5 and 1.5 models. The density of states

(DOS) and total energy calculation are treated with the $\boldsymbol{k}$-meshes increasing to the doubly fine

meshes for the optimized structure. The volume of the cell is optimized by the first-principles

calculation, assuming the original cubic-rock-salt lattice, by fitting the total energy as a function

of the volume to the Murnaghan's equation of state.[62] Three magnetic configurations, which are nonmagnetic (NM), ferromagnetic (FM), and C-and G-type antiferromagnetic (AFM) spin configurations of Mn, are considered for Li_2MnTiO_4. The FM configuration shows the most stable electronic structure, thus spin-polarized models are adopted for all models. The result is calculated using FM configuration hereinafter.

The first-principles calculation is also performed for a pure body-centered cubic (BCC) Li metal with space group $Im\bar{3}m$ and a solid O_2-molecule as the reference materials for the voltage-capacity profile and vacancy formation energies of Li and O. k-meshes of $16 \times 16 \times 16$ are adopted for Li, and optimized lattice constant is 3.364 Å, and k at the Γ point is adopted for the solid O_2-molecule with cubic supercells. The bond length with the lowest total energy for the solid O_2-molecule is estimated by fitting to a Lennard-Jones type potential.

3.3   Results and Discussion

3.3.1   Structural Stability

The optimized lattice constants of the $Li_{2-y}MTiO_4$ (M = V, Cr, Mn, Fe, Co, and Ni) structural models for $y = 0, 0.5, 1, 1.5$, and 2, are listed in Table 3.2. The optimized lattice constants are al-

Table 3.2: Optimized lattice parameters $a = b = c$ (Å) of the $Li_{2-y}MTiO_4$ (M = V, Cr, Mn, Fe, Co, and Ni) models for $y = 0, 0.5, 1, 1.5$, and 2.

y	$Li_{2-y}VTiO_4$	$Li_{2-y}CrTiO_4$	$Li_{2-y}MnTiO_4$	$Li_{2-y}FeTiO_4$	$Li_{2-y}CoTiO_4$	$Li_{2-y}NiTiO_4$
0	4.006	4.003	4.008	3.994	3.972	3.977
0.5	3.969	3.958	3.967	3.950	3.939	3.944
1	3.930	3.918	3.926	3.916	3.908	3.918
1.5	3.897	3.878	3.888	3.886	3.880	3.892
2	3.868	3.842	3.848	3.850	3.847	3.864

most independent of M and are consistent within 0.1 Å. The optimized lattice constant decreases with increasing y, reflecting the fact that the cell shrinks, because Li atoms are removed from the cathode for the charge reaction process. Experimental lattice constants except for Li_2CrTiO_4 were reported as 4.14 Å for Li_2VTiO_4,[35] 4.17-4.23 Å for Li_2MnTiO_4,[31,41] 4.17-4.18 Å for Li_2FeTiO_4,[31,34] 4.14-4.16 Å for Li_2CoTiO_4,[31,36] and 4.11-4.15 Å for Li_2NiTiO_4,[31,32,37–39]

showing little M-dependences, in agreement with calculated results. The optimized lattice constants are in good agreement with the experimental values within 5 % accuracy, although underestimate with the experiments. This underestimate is a consequence of the well-known drawbacks of LDA calculations, which usually underestimate lattice constants because atomic binding energies are overestimated.[15]

Relative volume change (RVC) during the charge and discharge reactions is a good indicator for evaluating the cycle performances, which is one of the most important factors for the rechargeable batteries[63]. The calculated RVC is shown in Fig. 3.2. Calculated RVC of
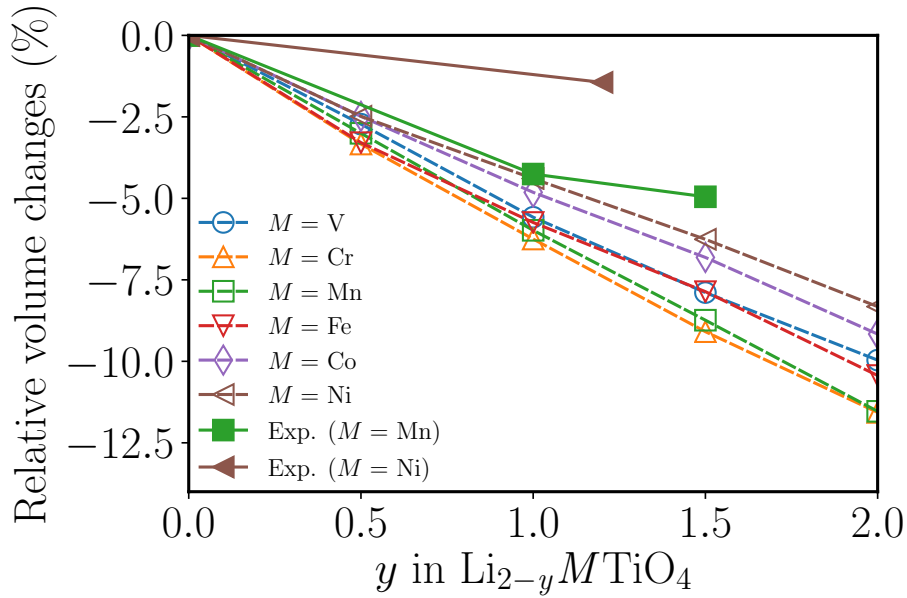
Figure 3.2: Calculated RVC (%) of $Li_{2-y}MTiO_4$ (M = V, Cr, Mn, Fe, Co, and Ni) for y = 0, 0.5, 1, 1.5, and 2. Blue circles, orange upward triangles, green squares, red downward triangles, purple diamonds, and brown left triangles show M = V, Cr, Mn, Fe, Co, and Ni, respectively. Experimental values are also plotted as solid green squares and solid brown left triangles for Li_2MnTiO_4[41] and Li_2NiTiO_4,[38] respectively.

$Li_{2-y}MTiO_4$ as a function of the Li deficiency y relative to the equilibrium volume of the Li_2MTiO_4 is defined as

$$\text{RVC}(y) = \frac{\Omega(Li_{2-y}MTiO_4) - \Omega(Li_2MTiO_4)}{\Omega(Li_2MTiO_4)}, \quad (3.16)$$

where $\Omega(X)$ is the equilibrium volume of X. The largest RVSs are found for M = Cr and

Mn, followed by Fe, V, Co, then Ni, and the tend of calculated RVCs for the element M is qualitatively in agreement with the experimental results, which were reported as 5 % in the case of M = Mn[41] and 1.5 % in the case of Ni.[38] These experimental RVCs suggested that both Li$_2$MnTiO$_4$ and Li$_2$NiTiO$_4$ are good cathode materials with the high cycle performances. This performances must be comparable to the low RVC of the olivine-type LiFePO$_4$, which shows small RVC of 6.8 %.[64] However, the experiment values were not obtained for the two-redox reaction, and there is only one experimental data for each of M = Mn and Ni. The calculated RVCs for all M are roughly 10 % in the assumption of the two-electron reaction, indicating that the cycle performances of the oxides are not so good in the two-electron reaction. In addition, the calculated RVCs overestimate the experimental values because of the small cell size. These results suggest that more detailed analyses both experimentally and theoretically are required to evaluate the cycle performances of the oxides.

A theoretical reaction proceeds via thermodynamically stable structures. Stability of the intermediate production is evaluated by calculated formation enthalpies on the basis of the fully discharged and charged phases. The calculated formation enthalpy $\Delta H(y)$ of Li$_{2-y}M$TiO$_4$ as a function of the Li deficiency y is shown in Fig. 3.3. Here, $\Delta H(y)$ is defined as

$$\Delta H(y) = E(\text{Li}_{2-y}M\text{TiO}_4) - \frac{2-y}{2}E(\text{Li}_2M\text{TiO}_4) - \frac{y}{2}E(M\text{TiO}_4), \tag{3.17}$$

where $E(X)$ is the calculated total energy of X. The calculated $\Delta H(y)$ for M = V, Cr, and Fe shows convex hull curves, indicating that the charge and discharge processes can proceed from $y = 0$ to 2 via the intermediate productions of $y = 0.5$, 1, and 1.5. For M = Mn, Co, and Ni, $\Delta H(y)$ at $y = 1.5$ lies above the $\Delta H(y)$ convex hull curves, showing that $y = 1.5$ cannot be produced during the charge and discharge reaction processes and the reactions for M = Mn, Co, and Ni proceed from $y = 0$ to 2 skipped $y = 1.5$ models. The structure stability is strongly correlated with electronic structures near the Fermi level as discussed in Sect. 3.3.4.
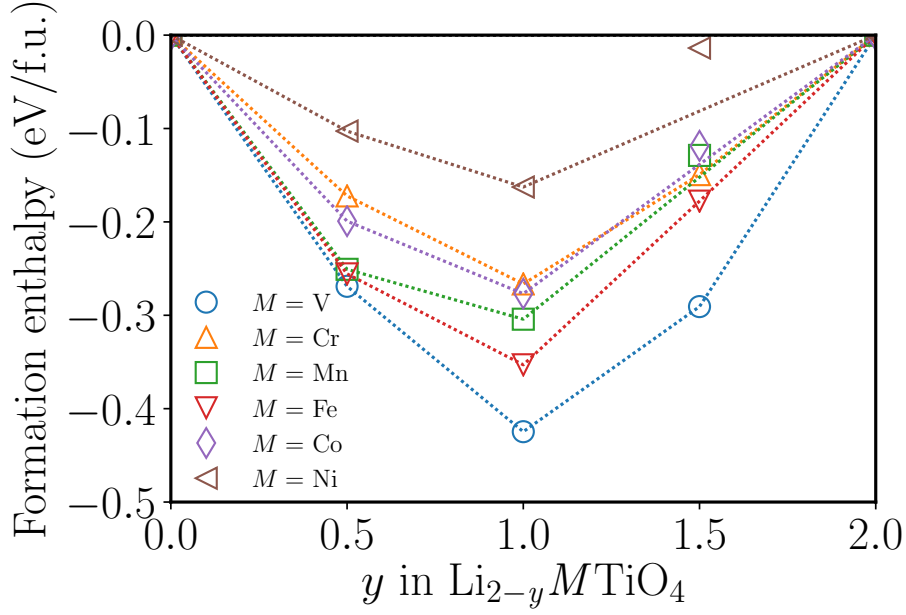
Figure 3.3: Calculated formation enthalpies of $\text{Li}_{2-y}M\text{TiO}_4$ (M = V, Cr, Mn, Fe, Co, and Ni) for y = 0, 0.5, 1, 1.5, and 2. Blue circles, orange upward-triangles, green squares, red downward-triangles, purple diamonds, and brown left-triangles show M = V, Cr, Mn, Fe, Co, and Ni, respectively, and most stable points are connected with dotted lines.

3.3.2 Voltage-Capacity Characteristics

The calculated and experimental voltage-capacity profiles of Li_2MTiO_4 (M = V, Cr, Mn, Fe, Co, and Ni) are shown in Fig. 3.4. The theoretical $V(y)$ is calculated, using Eq. (1.12), by

$$V(y) = -\frac{E(\text{Li}_{2-y+\Delta y}M\text{TiO}_4) - E(\text{Li}_{2-y}M\text{TiO}_4) - \Delta y E(\text{Li})}{\Delta y}, \tag{3.18}$$

where $E(y)$ is the calculated total energy of thermodynamically stable X.[13] The experimental $V(y)$ curves of Li_2MTiO_4 with cation-disordered rock-salt type structures were reported for M = V,[35] Mn,[41] Fe,[34] Co,[36] and Ni.[38]

The calculated $V(y)$ for all M decreases with decreasing y and lies in a range from 2.5 V to 5 V, similar to the experimental value. The experimental charge voltage is typically higher than the theoretical value because of an internal resistance in the battery cell. This internal resistance induces a voltage drop in the discharge reaction, thus the experimental discharge voltage is typically lower than the theoretical value. Therefore, the present calculated $V(y)$ is in
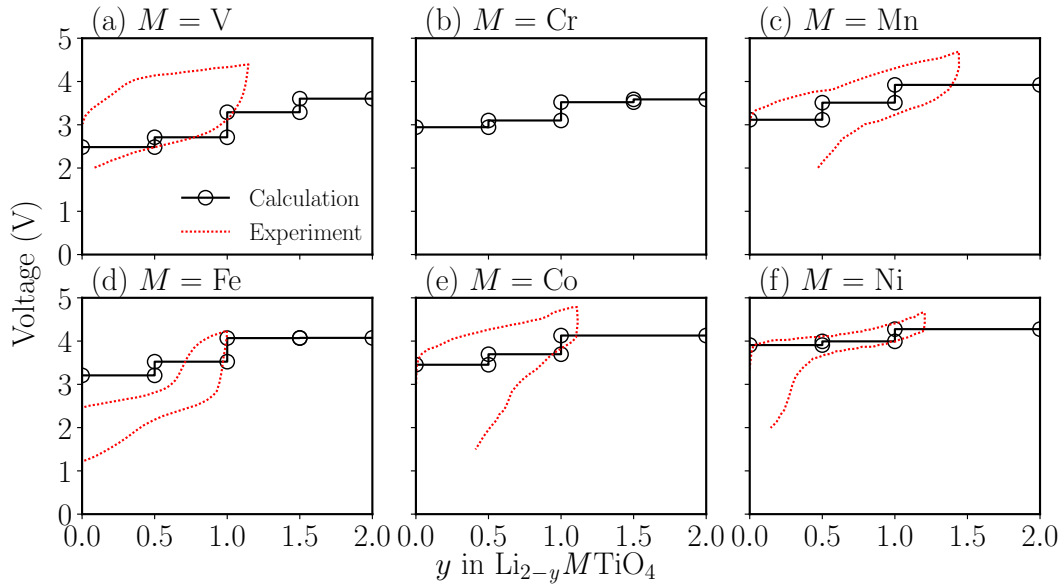
Figure 3.4: Calculated voltages of $Li_{2-y}MTiO_4$ as a function of the Li deficiency y for (a) M = V, (b) Cr, (c) Mn, (d) Fe, (e) Co, and (f) Ni are shown by black circles with solid lines. Experimental values of the initial charge and discharge for M = V,[35] Mn,[41] Fe,[34] Co,[36] and Ni[38] are plotted by red dotted lines.

good agreement with the experimental value, because the calculated $V(y)$ for all M is located on between the experimental charge and discharge voltages. As the number of $3d$ electrons in M increases, the calculated average voltage increases, and the voltage window decreases. The calculated $V(y)$ shows flat behavior especially for M = Co and Ni. In addition, the calculated $V(y)$ at $1 \leq y \leq 2$ for M = Mn and Fe has the almost same value with that at $0 \leq y \leq 2$ for M = Co and Ni. The voltage is strongly correlated with the redox reaction in the cathode, is discussed on the basis of the calculated electronic structure in Sect. 3.3.4.

3.3.3 Li- and O-Vacancy Formation Energies

As described in the introduction, the O_2-release, which degrades the battery system, is a serious problem, and the O_2-release from the Li_2MTiO_4 cathode was pointed out in the several experiments,[32, 37] contrary to the initial expectation.[41] In order to theoretically clarify the effect of the O_2-release from the cathode, the first principles calculation is performed for $Li_{2-y}MTiO_4$ with a single neutral O vacancy, and several Li- and O-vacancies are considered to evaluate the vacancy-site dependences by the calculations of Li- and O-vacancy formation energies.[65]

First, the formation energy $E[V_{Li}](y)$ of a single neutral Li vacancy (V_{Li}) per formula unit in $Li_{2-y}MTiO_4$ is defined by

$$E[V_{Li}](y) = E(Li_{(2-y)-1}MTiO_4) + E(Li) - E(Li_{2-y}MTiO_4), \qquad (3.19)$$

where $E(X)$ is the total energy of X and Li is treated as a pure metal with BCC structure. $E[V_{Li}](y)$ gives the same voltages as those obtained by Eq. (3.18) with $\Delta y = 1$ by the definition. Although the vacancy formation energy is generally defined as the energy difference between systems with and without vacancies, the above definition is adopted for evaluation of Li-vacancy formation energies to directly discuss defect stability in relation to the voltage. Second, the formation energy $E[V_O](y)$ of a single neutral O vacancy (V_O) per formula unit in $Li_{2-y}MTiO_4$ is defined as

$$E[V_O](y) = E(Li_{2-y}MTiO_3) + \frac{1}{2}E(O_2) - E(Li_{2-y}MTiO_4), \qquad (3.20)$$

assuming that O atoms are released from the cathode via O_2 molecule in accordance with the experiments.[32, 37] Finally, formation energy of the Li-vacancy $E[V_{Li} + V_O](y)$ in $Li_{2-y}MTiO_3$ ($Li_{2-y}MTiO_4$ with O vacancies) is also defined by combining Eq. (3.19) and (3.20) as

$$E[V_{Li} + V_O](y) = E(Li_{(2-y)-1}MTiO_3) + E(Li) - E(Li_{2-y}MTiO_3), \qquad (3.21)$$

and is consistent with the voltage of the O-deficient cathode material. The calculated Li- and O-vacancy formation energies $E[V_{Li}](y)$, $E[V_O](y)$, and $E[V_{Li} + V_O](y)$ as a function of the Li deficiency (y) are shown in Fig. 3.5.

The lowest O-vacancy formation energies are obtained in the model structures with O1 vacancy (see Table 3.1) for all M except for $M = V$, and the model structure with O3 vacancy for $M = V$ shows the lowest vacancy formation energy, which is 0.5 eV lower than that of the model structure with O1 vacancy. Six-ligand elements on O atoms are different for three sites, and the effective potential on O atoms produced by neighboring cations, which is the sum of
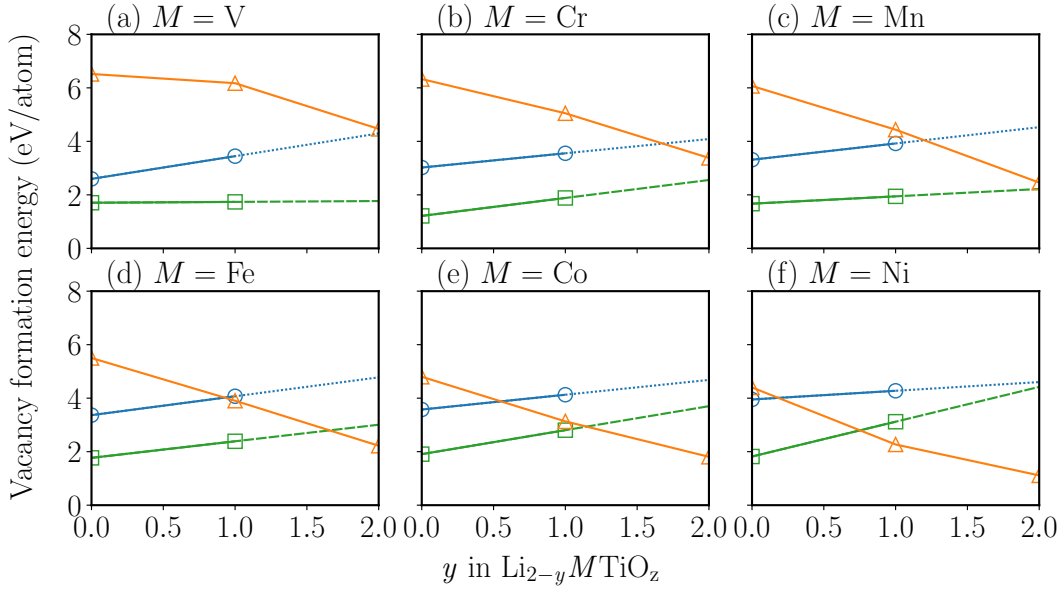
Figure 3.5: Calculated formation energies of Li and/or O vacancies (V_{Li} and V_O) in $Li_{2-y}MTiO_4$ for (a) M = V, (b) Cr, (c) Mn, (d) Fe, (e) Co, and (f) Ni are shown. Blue circles and orange triangles show the vacancy formation energies of V_{Li} and V_O, in $Li_{2-y}MTiO_4$, $E[V_{Li}](y)$ in Eq. (3.19) and $E[V_O](y)$ in Eq. (3.20), respectively. Green squares show the vacancy formation energies of V_{Li}, in $Li_{2-y}MTiO_3$ ($Li_{2-y}MTiO_4$ with the V_O model), $E[V_{Li} + V_O](y)$ in Eq. (3.21). Calculated values are connected by lines and extrapolated by dotted and dashed lines.

the positive charges of cations surrounding O, decreases in the order of O1, O2, and O3 sites, assuming that an ionic representation $Li_2^+ M^{2+} Ti^{4+} O_4^{2-}$. This is because the number of cations as O ligands are $4Li^+ + 2M^{2+}$ at O1, $4Li^+ + 2Ti^{4+}$ at O2, and $2Li^+ + 2M^{2+} + 2Ti^{4+}$ at O3. Therefore, it is expected that O1 site will be strongly affected by the Li removals during the charge reaction process. The calculated vacancy formation energy for all M shows that $E[V_{Li}](y)$ and $E[V_O](y)$ decrease and increase as y increases, respectively, indicating that Li and O are hardly and easily released from the cathode at the high charged phase, respectively. The magnitude of $E[V_O](y)$ depends on M and decreases with increasing number of $3d$ electrons as M changes from V to Ni. There exists an intersection between the $E[V_{Li}](y)$ and $E[V_O](y)$ lines, and the crossing point y_c also decreases with increasing number of $3d$ electrons as M changes from V to Ni. This result indicates that O can be released from the cathode more easily than Li in the y range higher than the critical point y_c.

A tendency of the calculated vacancy formation energy for M is found in Fig. 3.5. The

O_2-release from the cathode for $M = V$ is negligible because $E[V_O](y)$ is always higher than $E[V_{Li}](y)$ in the whole range of y. In contrast, for other M, $E[V_O](y)$ becomes lower than $E[V_{Li}](y)$ at the critical y points (y_c) and higher y, showing that O_2-release can take place much more easily than the Li-release at the critical y points (y_c) and the higher-y region. $E[V_O](y)$ for especially $M = Ni$ is lower than $E[V_{Li}](y)$ in the early reaction stage from y_c of about 0.2 and higher, because $E[V_O](y)$ decreases with increasing number of 3-d electrons as M changes from V to Ni, indicating that the O_2-release from the cathode is more appreciable in Li_2NiTiO_4. This result can explain well why the O_2-release was experimentally detected for $M = Ni$ at high voltages. Experimental voltage-capacity profiles are mostly measured by setting the potential window up to about 4-5 V owing to the limitation of the stability of the organic electrolyte, and the calculated $E[V_{Li}](y)$ approaches or crosses with this experimental upper potential-window region as y increases. Therefore, the maximum rechargeable capacities are practically limited to less than that of the two-electron reaction.

The calculated $E[V_{Li} + V_O](y)$ is always lower than $E[V_{Li}](y)$ in the whole y range, showing that Li is easily released from the O-deficient cathode than those without O vacancies, because by the definition $E[V_{Li}](y)$ and $E[V_{Li} + V_O](y)$ correspond to the voltage of the cathodes with and without O vacancies, respectively. Therefore, the O_2-release can degrade the battery performances in terms of the voltage, especially for late-transition metals $M = Co$ and Ni. Note that the dynamics of O in the cathode remain to be clarified in future studies.

3.3.4 Electronic Structures

The energetic analyses of V_O and V_{Li} show that the tend of the O_2-release is strongly correlated to the M element and the Li-deficiency y, but the detailed mechanism of the O_2-release is not clarified yet. In this section, the representative case of $M = Mn$, which has the critical point y_c at about $y_c = 1$, is focused, and the microscopic reaction mechanism and the structural stability are discussed on the basis of the calculated electronic structures.

Figure 3.6 shows the calculated total and partial DOSs (TDOSs and PDOSs) of $Li_{2-y}MTiO_4$ with $y = 0, 1, 2$. The PDOSs are shown by decomposing into the components of symmetry-

inequivalent sites. The calculated TDOSs for all y show metallic electronic structures, although
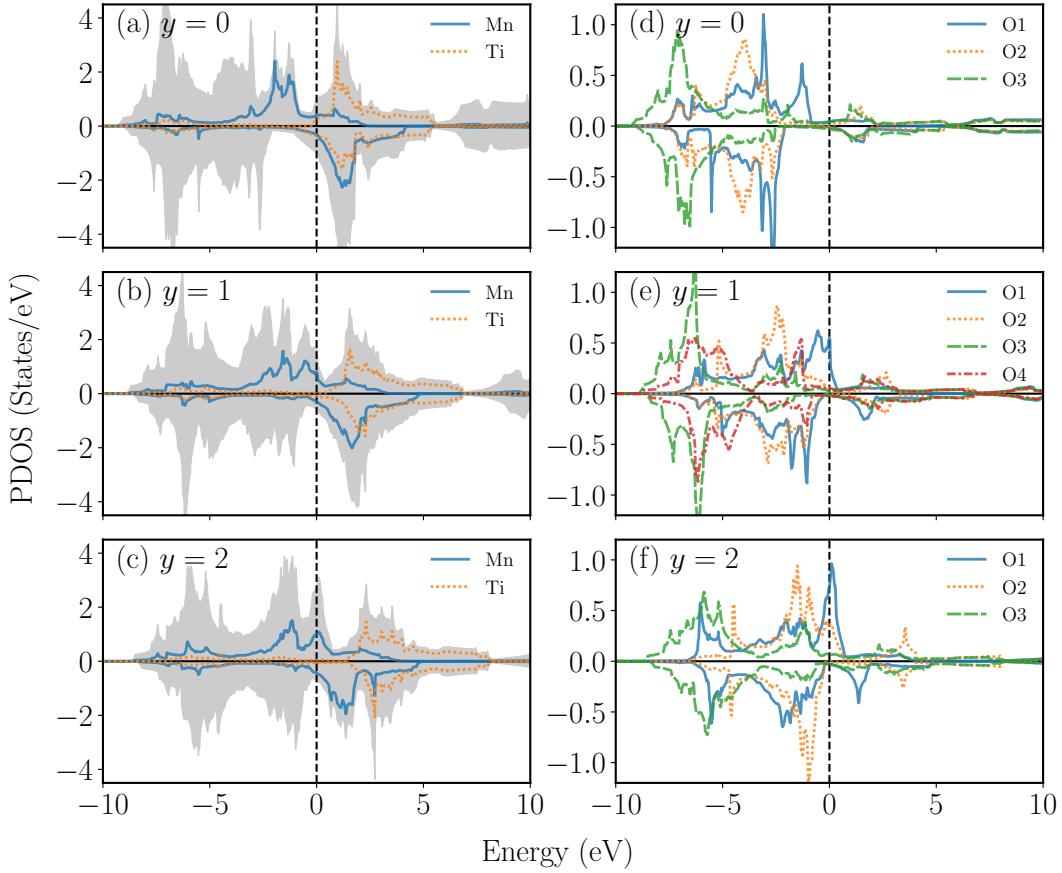
Figure 3.6: Calculated total densities of states (TDOSs) of $Li_{2-y}MnTiO_4$ for (a) $y = 0$, (b) $y = 1$, and (c) $y = 2$ are shown by gray hatched regions. Calculated partial densities of states (PDOSs) projected on Mn and Ti are potted by solid blue and dotted orange lines, respectively. Calculated PDOSs of $Li_{2-y}MnTiO_4$ projected on symmetrically inequivalent O sites O1, O2, O3, and O4 are shown by solid blue, dotted orange, dashed green, and dash-dotted red lines, respectively, for (d) $y = 0$, (e) $y = 1$, and (f) $y = 2$. The Fermi levels are indicative by vertical dashed lines.

the oxides, such as Li_2MnTiO_4, have generally considered to be insulators. Thus LDA+U calculations are performed on Li_2MnTiO_4 to include strong correlations of localized d electrons, $U = 5$- 12 eV for Mn and Ti is used. The effect of structural distortions such as the JT distortions with respect to c/a is also taken into account, because Li_2MnTiO_4 in high spin state may have a band gap, assuming Mn^{2+} ($3d^5$). However, the calculated DOSs of Li_2MnTiO_4 with $U = 5$ and 8 eV show metallic electronic structures too, furthermore, the effect of U on the TDOS gives negligibly small differences. A large value of $U = 12$ eV, which is much larger than typical U values adopted in previous reports,[46, 48] is required to open the band gap, thus results without

U are discussed bellow.

The calculated TDOS for $y = 0$ shows low electronic states around the Fermi level, but the electronic structure shifts to high energy region with respect to the Fermi level. Consequently, electronic states near the Fermi level become increasing as y increases, because electrons are removed from the occupied valence states on the Li removals. As a result, the DOS for $y = 2$ has a sharp peak at the Fermi level in the up-spin TDOS, and for $y = 1$ there exists the high peak at slightly below the Fermi level. The TDOSs at high energy conduction band regions around 10 eV are mainly composed of Li-$2s$ states, indicating that Li exists as Li^+ ion in the cathode. Electronic structures processing a high DOS at the Fermi level imply that systems are energetically unstable. In fact, the calculated formation enthalpy shows that the reaction intermediate at $y = 1.5$ cannot be produced stably during the charge and discharge reaction processes.

The calculated PDOSs of Li_2MnTiO_4 ($y = 0$) shown in Fig. 3.6 (a) and 3.6 (d) indicate that low energy regions of the valence bands mainly consist of O states and the high energy regions of the valence and conduction states are mainly composed of Mn and Ti states. This indicates that O basically has the typical O^{2-} ionic sates for $y = 0$. The PDOS of Mn for $y = 0$ shows that the up- and down-spin states are roughly fully occupied and unoccupied, respectively, corresponding to the Mn^{2+} ($3d^5$) ionic picture. Similarly, the PDOS of Ti for $y = 0$ shows the almost unoccupied Ti^{4+} ($3d^0$) electronic configuration. The result shows that the calculated electronic structure can be understood as the ionic representation of $Li_2^+Mn^{2+}Ti^{4+}O_4^{2-}$, but to be precise, there exist slight differences from the rigid-ion model due to effect of hybridization as seen in the PDOSs.

Assuming the stoichiometric reaction mechanism of Li_2MTiO_4, M^{2+}/M^{3+}- and M^{3+}/M^{4+}-redox reactions proceed as y increases from 0 to 2. However, the previous experiments suggested that the elements other than *M* have non-negligibly contributions to the battery reaction. The calculated DOSs indicate a significant role of the contribution of O to the battery reaction, in addition to the roles of *M*, supporting the previous experiments.[41] As expected from the stoichiometric representation, the up-spin states of Mn shift to a higher energy with respect

to the Fermi level with increasing y, and electrons are removed from the Mn-occupied states. This can be approximating as the redox-reaction from $Mn^{3+}(3d^4)$ in $LiMnTiO_4$ to $Mn^{4+}(3d^3)$ in $MnTiO_4$. The PDOSs of Ti also shift to a higher energy region with respect to the Fermi level as y increases while keeping the $Ti^{4+}(3d^0)$ states. However, to be precise, there exists a small mixing of Ti with the valence band, which is presented by of $Ti^{(4-\delta)+}$ in $y = 0$. The mixing decreases as y increases, indicating that the ionic valence of Ti changes form $Ti^{(4-\delta)+}$ to Ti^{4+}. Therefore, the Ti-redox reaction has a minor contribution to the battery reaction. This minor effect on the battery reaction was observed in several experiments.[36,38] Similarly, the change in the calculated PDOS of Mn is smaller than that predicted by the stoichiometric reaction, considering that the changes in the PDOS of Mn with y are not large enough to realize the nominal ionic valence. This is because the O states significantly change as y increases, and the O-redox reaction dominantly contributes to the battery reaction especially at late charging reaction process.

The PDOSs of O shift to a higher energy with respect to the Fermi level with hole doping in the occupied states as y increases, indicating that significant contribution of the O-redox reaction to the battery reaction especially in the $1 \leq y \leq 2$. The PDOSs of O for $y = 1$ and 2 have high peaks around the Fermi levels, thus the high peaks seen in the TDOSs, which make the systems unstable, are predominantly associated with the O states, supporting the instability of $y = 1.5$ shown by the calculated formation enthalpies. Furthermore, the calculated vacancy formation energy also shows the degradation of the structural stability at the late charged phases and the tend of the easier O_2-release from the cathode as y increases. As seen in Figs. 3.6 (e) and 3.6 (f), the high peaks around the Fermi levels are mainly composed of the O1 states, and calculated electronic structures of $Li_{2-y}MTiO_3$ with O1 vacancy indicate disappearing these peaks, inducing the lower V_O formation energies at higher y.

The microscopic charge and discharge reaction mechanism in Li_2MnTiO_4 cathodes is discussed on the basis of the above findings, being associated with two types of redox reactions depending Li concentration in the cathode by the calculated electronic structure changes. The Mn-redox reaction predominates with the minor contribution of the Ti-redox reaction in the

lower y regions (roughly $0 \leq y \leq 1$), and the both Mn- and O-redox reactions can take place in the higher y regions (roughly $1 \leq y \leq 2$). This result supports the recent experimental results.[41]

In above paragraphs, the microscopic charge and discharge reaction mechanism for $M =$ Mn was focused and discussed on the basis of the calculated electronic structures, and in the following paragraphs, the effect of M on the reaction mechanisms is discussed. The calculated TDOSs and PDOSs of $M =$ V, Cr, Fe, Co, and Ni are shown in Fig 3.8, 3.9, 3.10, 3.11, and 3.12, respectively, in the following appendix. As the number of $3d$ electrons in M increases as M changes from V to Ni, the calculated DOSs show that the energy level of M-$3d$ states decreases with respect to the Fermi level in contrast those of the O-$2p$ states, which relatively increase, inducing the high peak originating from O1 around the Fermi level at lower y region as the number of $3d$ electrons in M increases. This M dependence on the electronic structures can explain the M dependence of the critical point y_c, which was discussed for the calculated Li- and O-vacancy formation energies, indicating that the stability of Li_2MTiO_4 during the charge and discharge reaction processes becomes decreasing as the number of $3d$ electrons in M is changed. The calculated DOSs for $M =$ V show that the O states always lie below the Fermi levels in the whole y regions, suggesting that the O-redox reaction does not occur. The contribution of the O-redox reaction to the battery reaction become stronger as increasing number of $3d$ electrons in M is changed, especially from Mn to Ni, inducing flatter voltage-capacity characteristics. The calculated voltages independent of M are about 4 V at higher than y_c, and the width of the potential window decreases as M changes from Mn to Ni. This result suggests that the O-redox potential is about 4 V and the O-redox reaction predominates in these oxides for the cathode materials.

3.3.5 Effects of Transition Metals on the Battery Reaction

The microscopic reaction mechanism of Li_2MTiO_4 ($M =$ V, Cr, Mn, Fe, Co, and Ni) depending on M is systematically understood by the calculated electronic structure, and the structural stability against the O_2-release from the Li_2MTiO_4 cathode is also evaluated by the calculating

Li- and O-vacancy formation energies. In this section, by showing the overall reactions of the Li$_2M$TiO$_4$ cathode, the effect of transition metals on the battery reaction including the O$_2$-release is discussed and the best candidate for the cathode material will be proposed on the basis of the above findings. Figure 3.7 shows the calculated voltage and the y_c value for the O$_2$-release. The lower limit of the calculated voltage increases as M changes from V to Ni, although
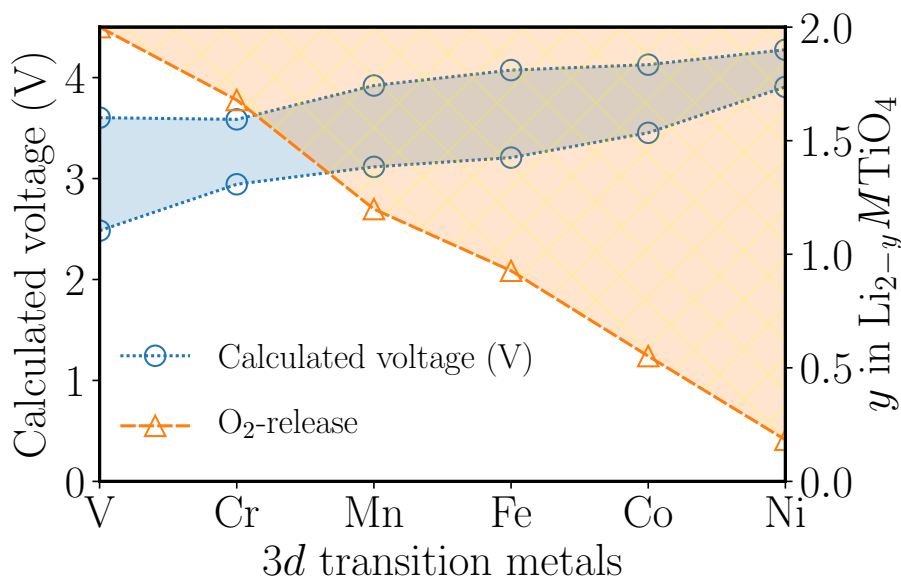
Figure 3.7: Upper limits and lower limits of calculated voltages of Li$_{2-y}M$TiO$_4$ are shown by blue circles with dotted lines. Evaluated critical Li deficiency y_c in Li$_{2-y}M$TiO$_4$ are shown by orange triangles with a dashed line. The calculated vacancy formation energies of O are lower than those of Li in the orange hatched area, which is in the y range higher than y_c.

the upper limit of them is almost same for M = Mn, Fe, Co, and Ni. This result indicates that M = Ni can achieve the higher voltage and smaller voltage fluctuation than other M elements. However, y_c for the O$_2$-release decreases as M changes from V to Ni, and M = V shows the highest structural stability against the O$_2$-release. Therefore, the high voltage and high structural stability against the O$_2$-release compete with each other and unfortunately cannot be satisfied at the same time. Although Li$_2$VTiO$_4$ shows the highest structural stability against the O$_2$-release in a wide range y, its voltage is relatively lower than those of the typical commercialized Li-ion batteries. In contrast, Li$_2$MnTiO$_4$ shows the adequate voltage-capacity characteristics for the commercial use, although the effect of the O$_2$-release cannot be negligible at y higher than

about 1.25. Li_2NiTiO_4 has the highest voltage, although the O_2-release is appreciable even in the early charged stages of about $y \geq 0.2$. Therefore, The best choice for the cathode material in the trade-off is Li_2CrTiO_4, which is satisfied with both high voltage and high structural stability against the O_2-release. To my best knowledge, experimental results for Li_2CrTiO_4 cathode have not been reported, thus future experimental studies are required to discuss with the present calculation.

3.4 Conclusion

The phase stability for different Li concentrations, the voltage-capacity characteristics, the Li- and O-vacancy formation energies, and the electronic structures of $Li_{2-y}MTiO_4$ (M = V, Cr, Mn, Fe, Co, and Ni) for y = 0, 0.5, 1, 1.5, and 2 were investigated by the first-principles calculation. The calculated voltage-capacity characteristics show that the voltage increases and the width of potential window becomes narrow as the number of $3d$ electrons in M is increased. The O_2-release from the cathode becomes significant at the low Li concentration in the cathode, and the structural stability against the O_2-release decreases as M changes in the oxides from V to Ni. Therefore, the materials containing the large number of $3d$ electrons, such as Li_2CoTiO_4 and Li_2NiTiO_4, achieve high voltages, while the structural stability against the O_2-release is lower than that of other M elements. The atomistic stability against the O_2-release is well-explained on the basis of the calculated electronic structures, which shows the correlation with the positions of energy levels of O-$2p$ in the DOSs. The voltage and the structural stability against the O_2-release are in a trade-off relationship, and it is expected that Li_2CrTiO_4 is a good candidate for the cathode use.

3.5 Appendix

The calculated TDOSs and PDOSs of M = V, Cr, Fe, Co, and Ni are shown in Fig 3.8, 3.9, 3.10, 3.11, and 3.8, respectively.
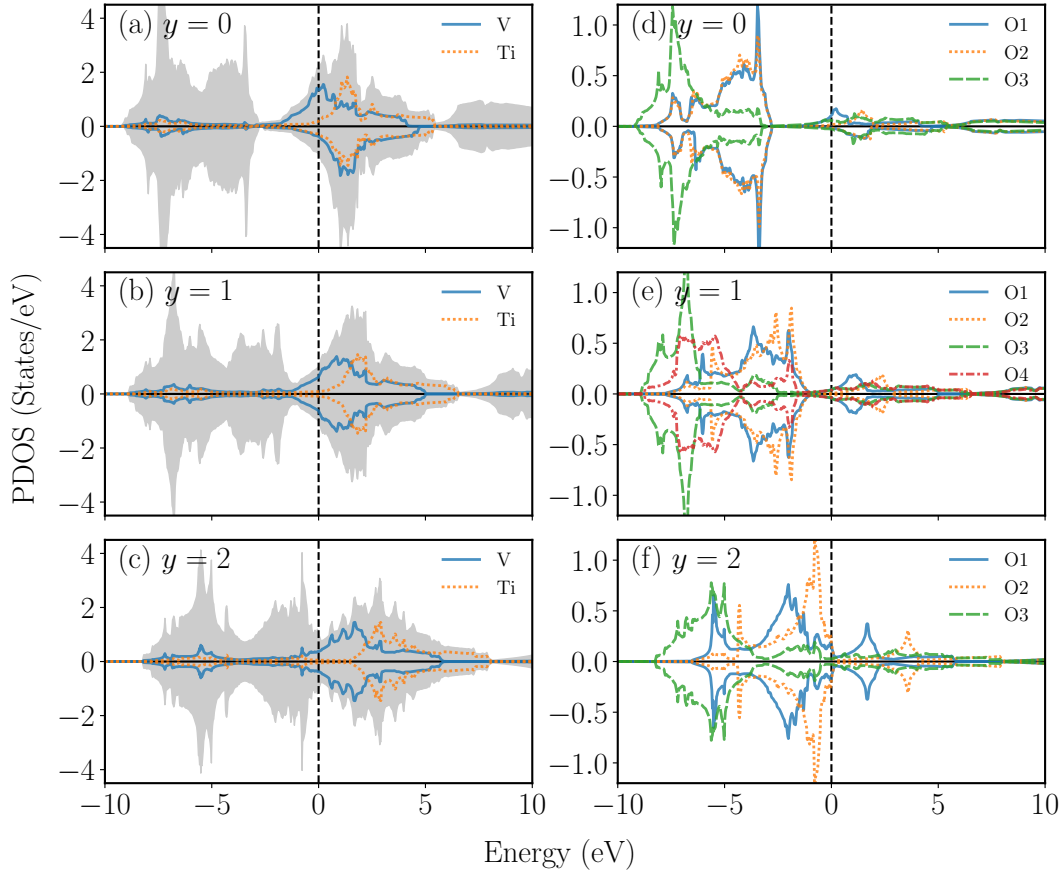
Figure 3.8: Calculated total densities of states (TDOSs) of $Li_{2-y}VTiO_4$ for (a) $y = 0$, (b) $y = 1$, and (c) $y = 2$ are shown by gray hatched regions, and calculated partial densities of states (PDOSs) projected on V and Ti are potted by solid blue and dotted orange lines, respectively. Calculated PDOSs of $Li_{2-y}VTiO_4$ projected on symmetrically inequivalent O sites O1, O2, O3, and O4 are shown by solid blue, dotted orange, dashed green, and dash-dotted red lines, respectively, for (d) $y = 0$, (e) $y = 1$, and (f) $y = 2$. The Fermi levels are indicative by vertical dashed lines.
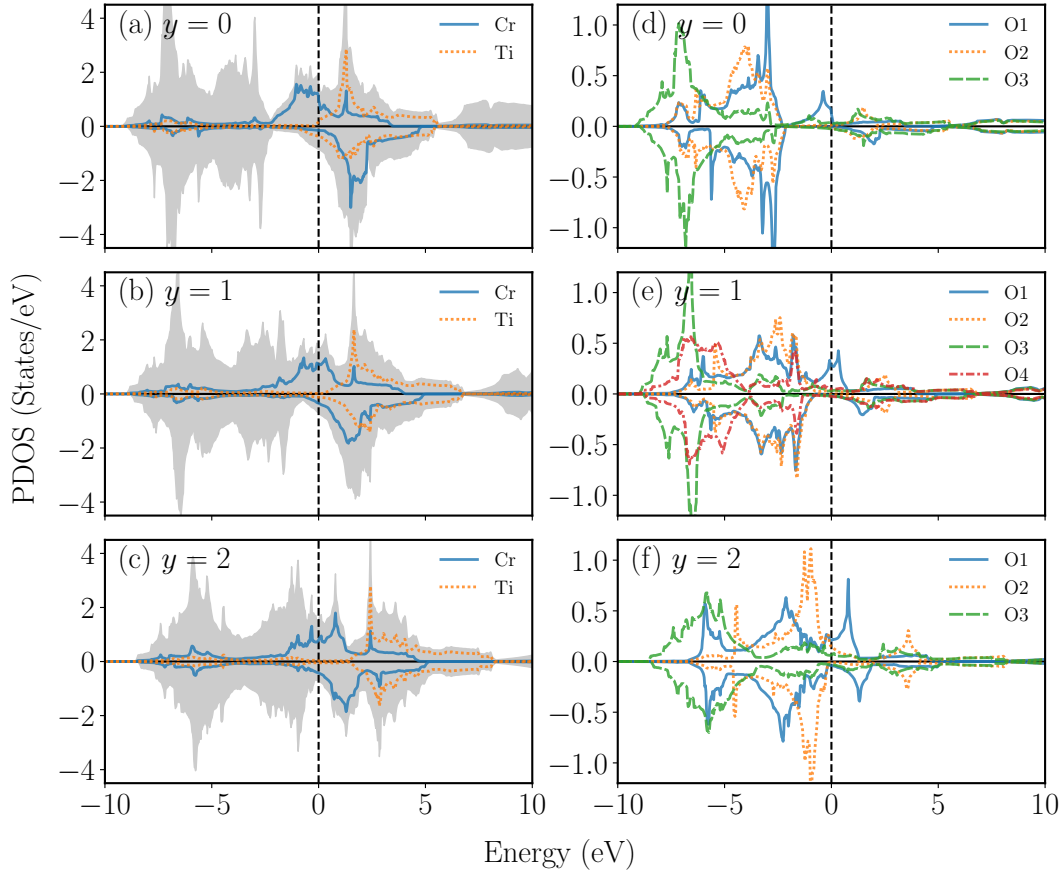
Figure 3.9: Calculated total densities of states (TDOSs) of $Li_{2-y}CrTiO_4$ for (a) $y = 0$, (b) $y = 1$, and (c) $y = 2$ are shown by gray hatched regions, and calculated partial densities of states (PDOSs) projected on Cr and Ti are potted by solid blue and dotted orange lines, respectively. Calculated PDOSs of $Li_{2-y}CrTiO_4$ projected on symmetrically inequivalent O sites O1, O2, O3, and O4 are shown by solid blue, dotted orange, dashed green, and dash-dotted red lines, respectively, for (d) $y = 0$, (e) $y = 1$, and (f) $y = 2$. The Fermi levels are indicative by vertical dashed lines.
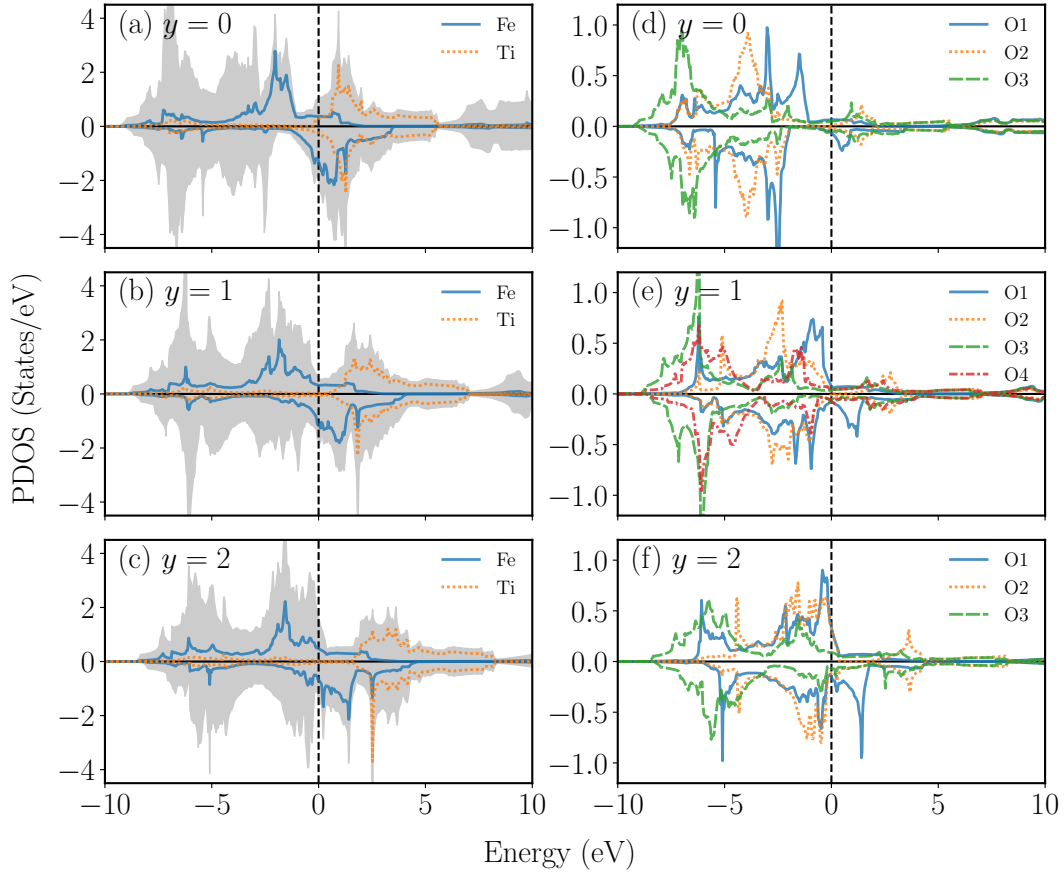
Figure 3.10: Calculated total densities of states (TDOSs) of Li$_{2-y}$FeTiO$_4$ for (a) $y = 0$, (b) $y = 1$, and (c) $y = 2$ are shown by gray hatched regions, and calculated partial densities of states (PDOSs) projected on Fe and Ti are potted by solid blue and dotted orange lines, respectively. Calculated PDOSs of Li$_{2-y}$FeTiO$_4$ projected on symmetrically inequivalent O sites O1, O2, O3, and O4 are shown by solid blue, dotted orange, dashed green, and dash-dotted red lines, respectively, for (d) $y = 0$, (e) $y = 1$, and (f) $y = 2$. The Fermi levels are indicative by vertical dashed lines.
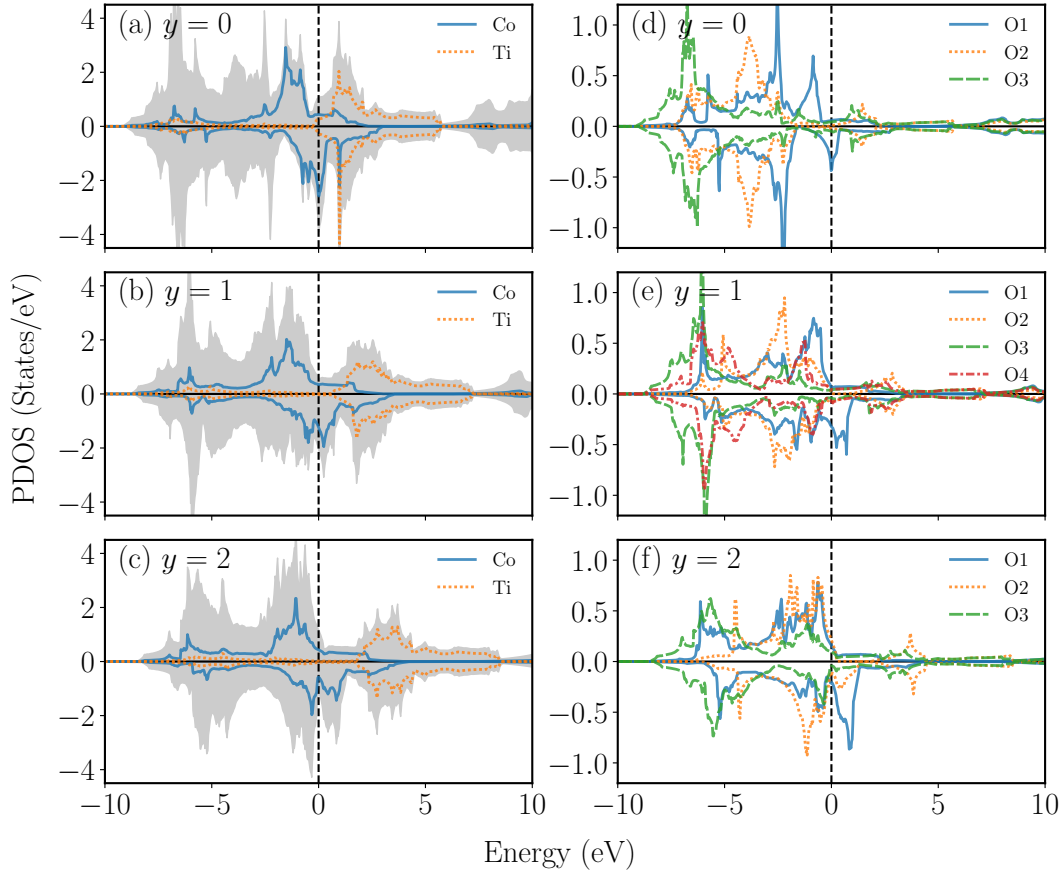
Figure 3.11: Calculated total densities of states (TDOSs) of $Li_{2-y}CoTiO_4$ for (a) $y = 0$, (b) $y = 1$, and (c) $y = 2$ are shown by gray hatched regions, and calculated partial densities of states (PDOSs) projected on Co and Ti are potted by solid blue and dotted orange lines, respectively. Calculated PDOSs of $Li_{2-y}CoTiO_4$ projected on symmetrically inequivalent O sites O1, O2, O3, and O4 are shown by solid blue, dotted orange, dashed green, and dash-dotted red lines, respectively, for (d) $y = 0$, (e) $y = 1$, and (f) $y = 2$. The Fermi levels are indicative by vertical dashed lines.
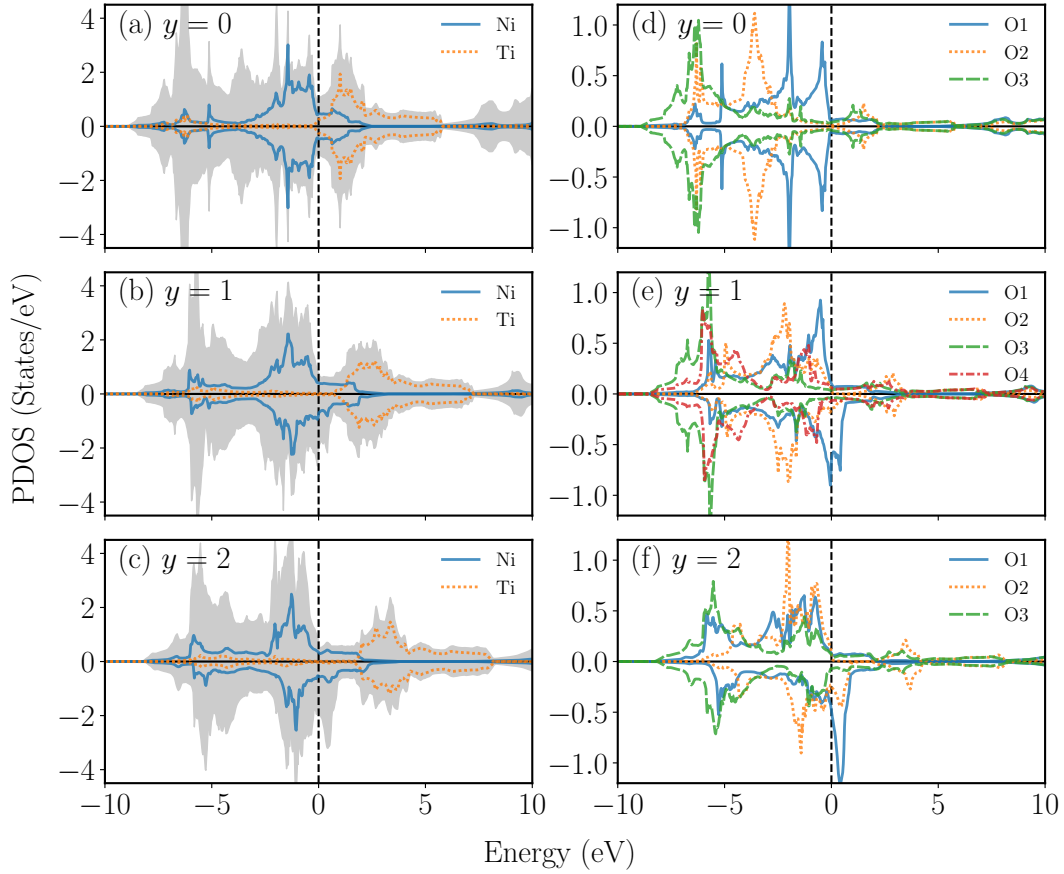
Figure 3.12: Calculated total densities of states (TDOSs) of $Li_{2-y}NiTiO_4$ for (a) $y = 0$, (b) $y = 1$, and (c) $y = 2$ are shown by gray hatched regions, and calculated partial densities of states (PDOSs) projected on Ni and Ti are potted by solid blue and dotted orange lines, respectively. Calculated PDOSs of $Li_{2-y}NiTiO_4$ projected on symmetrically inequivalent O sites O1, O2, O3, and O4 are shown by solid blue, dotted orange, dashed green, and dash-dotted red lines, respectively, for (d) $y = 0$, (e) $y = 1$, and (f) $y = 2$. The Fermi levels are indicative by vertical dashed lines.

Part III

Significant Role of Oxygen-redox Reaction with O_2-Release in Li-Excess Cation-Disordered Rock-Salt Cathodes $Li_{2+2x}Mn_{1-x}Ti_{1-x}O_4$ for the Li-Ion Battery

4.1 Introduction

The oxides of the cation-disordered rock-salt type have been expected to be alternative candidates for the conventional cathode materials. In the previous part, the effect of the $3d$-transition metals on the battery reaction was focused, and $Li_2M TiO_4$ (M = V, Cr, Mn, Fe, Co, and Ni) of rock-salt type was investigated by the first-principles calculation. The battery reaction mechanism is mainly associated with the M- and O-redox reactions depending on the Li concentration in the cathode. The O_2-release from the cathode, which has been observed experimentally,[32,37] was theoretically discussed, and the tend of O_2-release at low Li concentration increases with the O-redox reaction as the number of $3d$-electrons in M increases. The calculated voltage increases as M changes from V to Ni. Therefore, there is the trade-off relation between the voltage and the structural stability against the O_2-release. It was concluded that Li_2CrTiO_4 is the best candidate for the cathode material among the oxides on owing to its high voltage and high structural stability. However, Cr is highly toxic element and better to be avoided in commercial use.

Recently, experimental studies indicated that Li-excess phase, $Li_{2+2x}Mn_{1-x}Ti_{1-x}O_4$ with Li-excess x around 0.2, shows higher rechargeable capacity than that of the x = 0 phase.[41,46,47,66,67] Kitajou et al. electrochemically observed the battery performances of $Li_{2+2x}Mn_{1-x}Ti_{1-x}O_4$ cathodes with x = 0-0.3, and effects of x on the cathode properties were investigated. The measured maximum charge and discharge capacities correspond to 1.86- and 1.57-electron reaction for x = 0.3 and 0.2, respectively. These capacities are close to the theoretical ones of the reaction equation[41] written by

$$Li_{2+2x}Mn_{1-x}Ti_{1-x}O_4 \rightleftarrows Mn_{1-x}Ti_{1-x}O_4 + (2 + 2x)Li. \qquad (4.22)$$
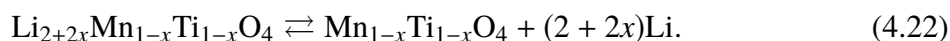
It was also suggested that Mn- and O-redox couples predominantly contribute to charge compensations in early and late charging processes, respectively, by XANES measurements. Yabuuchi et al. reported experimentally that the $Li_{2.4}Mn_{0.8}Ti_{0.8}O_4$ (x = 0.2) cathode shows rechargeable capacity exceeding 300 mAh/g, originating from less covalency between Mn-d and O-p states in

comparison with $Li_{1.3}Nb_{0.3}Fe_{0.4}O_2$.[46] However, the effect of x in $Li_{2+2x}Mn_{1-x}Ti_{1-x}O_4$ on the battery performances has not been systematically clarified yet, and understandings of x-effects in the cathodes might help to design the new cathode materials with high capacities and high voltages.

In this part, cathode properties of $Li_{2+2x}Mn_{1-x}Ti_{1-x}O_4$ ($0 \leq x \leq 0.3$) are investigated by first-principles calculation in order to clarify the effects of x on the battery performances. To evaluate the structural stability and the microscopic reaction mechanism in the cathode materials for each x, formation enthalpies of $Li_{2+2x}Mn_{1-x}Ti_{1-x}O_4$ are calculated as a function of the Li-deficiency y considering several configurations of Li sites. Based on the estimated theoretical reaction processes, the voltage-capacity characteristics are obtained for each x and compared with the experimental results. The roles of cation- and anion-redox reaction couples depending on y as well as x are discussed in detail by analyzing calculated electronic structures. Energy stability of the O_2-release from the cathodes is discussed theoretically by calculating vacancy formation energies of Li and O. On the basis of the findings of calculations, the best x values on owing to the voltages, capacities, and structural stability against the O_2-release are discussed and proposed.

4.2   Models and Method

Supercell models for $Li_{2+2x}Mn_{1-x}Ti_{1-x}O_4$ with the rock-salt-based structures are adopted for the fully charged pristine states for $x = 0, 0.1, 0.2$, and 0.3, as shown in Fig. 4.1. The model includes 80 atoms/cell in the $\sqrt{5} \times \sqrt{5} \times 2$ cell of the conventional rock-salt based unit cell, which is used in the Sect. 3.2 in the Part II to study Li_2MTiO_4. In order to reproduce disorder of cation sites in the finite-size cell, the special quasi-random structure (SQS) method,[68] which is implemented in the Alloy-Theoretic Automated Toolkit (ATAT) code,[69,70] is adopted for the supercell model. In the SQS method, atomic positions are determined so that correlation functions of elements randomly distributed in the cell approach those in an ideal random cell.[68] Li atoms are removed from the pristine models ($y = 0$) by finding atomic-site configurations with lower Madelung
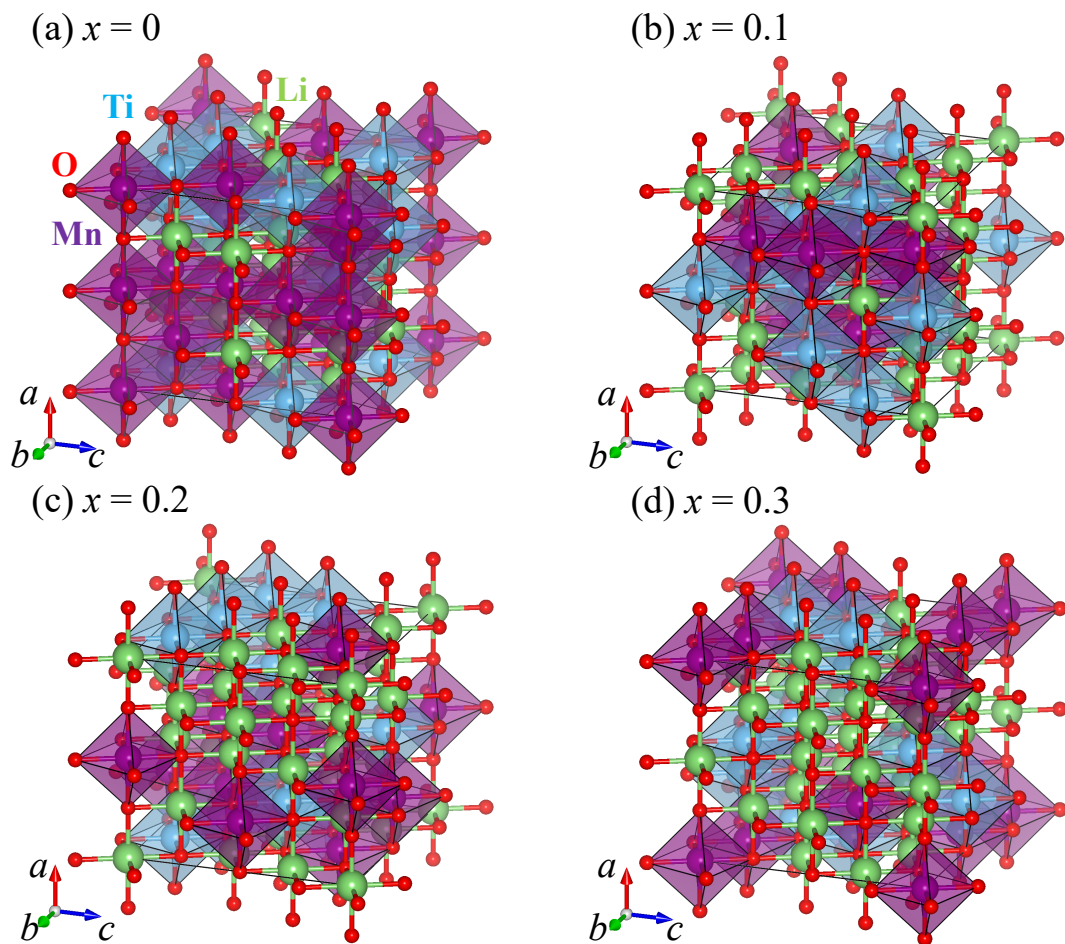
Figure 4.1: Calculated model structures of $Li_{2+2x}Mn_{1-x}Ti_{1-x}O_4$ for (a) $x = 0$, (b) 0.1, (c) 0.2, and (d) 0.3 as fully-discharged phases. Green, purple, blue, and red spheres show Li, Mn, Ti, and O, respectively. These figures were visualized by VESTA.[6]

energies among possible Li (or Li vacancy) configurations using the supercell program.[71] Here, atomic positions of Mn and Ti are kept to those at $y = 0$ to consider the Li-intercalations reaction because the XRD measurements showed that the rock-salt type structures maintain during the charge and discharge reaction processes.[41] Five candidate models for each y with the lowest Madelung energies are selected, and the atomic structures and volumes of these structure models are fully optimized by first-principles calculations. Effects of cation-site configurations on the structural stability have been considered to be small for the systems including d^0 transition metals such as Ti^{4+}, because d^0 elements can tolerate distortions of cation sites with very low energy costs stabilizing the structure of the cation-disordered rock-salt type.[48]

The first-principles calculation is based on the DFT with generalized gradient approximation (GGA),[72] and the Hubbard correction (GGA+U) method is also used to include strong correlations among localized $3d$ electrons of transition metals.[73] The U_{eff} value of 3.90 eV is adopted for Mn-d orbitals.[74] The computations are performed using the Quantum ESPRESSO code,[75,76] based on the projector augmented wave (PAW) method,[77] and cut-off energies of 60 and 500 Ry are used for the wave functions and charge densities, respectively. The pslibrary ver. 0.3.1 is used as a pseudo-potential file set.[78] Atomic structures of the models are fully optimized until forces acting on every atom become at least smaller than 10 mRy/Bohr, and the $\boldsymbol{k}$-integrations are treated with the $\boldsymbol{k}$-mesh of $2 \times 2 \times 2$. Total energies of the optimized models are calculated with the improved tetrahedron method with the $\boldsymbol{k}$-mesh of $4 \times 4 \times 4$.[61] For models including O vacancies used to study the O_2-release from the cathodes, the $\boldsymbol{k}$-mesh of $2 \times 2 \times 2$ is used for both structure optimizations and total energy calculations.

In this part, all results are obtained by the calculation with GGA+U. For the $x = 0$ model in the previous part, energetically the most stable magnetic state is calculated to be the FM state compared to the NM and AFM states, and the results with the FM state is shown for all the model hereinafter.

4.3　Results and Discussion

4.3.1　Structural Stability

The lattice constants of $Li_{2+2x}Mn_{1-x}Ti_{1-x}O_4$ models calculated by the cell optimizations assuming cubic cells are 4.34, 4.27, 4.23 and 4.19 Å for $x = 0$, 0.1, 0.2, and 0.3, respectively, being in good agreement with the experimental values (4.2, 4.18, 4.17, and 4.16 Å for $x = 0$, 0.1, 0.2, and 0.3, respectively).[41] The calculations slightly overestimate the experimental values up to about 5 % at $x = 0$, consisting with a general trend of a GGA+U calculation.

As described in the previous part, RVC is an important index to estimate the cycle performances of the Li-ion batteries,[63] and the RVC of the $Li_{2+2x}Mn_{1-x}Ti_{1-x}O_4$ model as a function of y for each x is calculated, shown in Fig. 4.2. RVC is defined as

$$RVC_x(y) = [\Omega_x(y) - \Omega_x(0)]/\Omega_x(0), \tag{4.23}$$

where $\Omega_x(y)$ is the calculated equilibrium volume of $Li_{2+2x-y}Mn_{1-x}Ti_{1-x}O_4$. The result indicates basically that the volume decreases with increasing y, but the slope becomes smaller at roughly $y > 1$ in both calculations and experiments. The calculated RVCs of $x = 0 - 0.3$ are smaller than 10 % in the calculated y ranges, suggesting that these cathode materials can have good cycle characteristics especially in low y regions. The experimental RVCs of $Li_{2+2x-y}Mn_{1-x}Ti_{1-x}O_4$ were reported to be smaller than 5 % for $x = 0$ and 0.2,[41] consistent with the calculated results. Both calculations and experiments indicate a same trend of smaller RVCs for high x, supporting that the cycle performance can be improved in the Li-excess materials. However, an irregular behavior as typical RVCs is also confirmed in the calculated RVCs in $y > 0.5$ for $x = 0.3$, which shows that the volume increases as y increases. This is because significant structural rearrangements at cation sites around the open spaces formed with Li vacancies. In the high y regions for high x phases, the local atomic structures especially at Li and Mn largely change from octahedral to tetrahedral coordinates with O (*e.g.*, from dense LiO_6 to sparse LiO_4 polyhedral networks, respectively). Such lowered coordination numbers

59
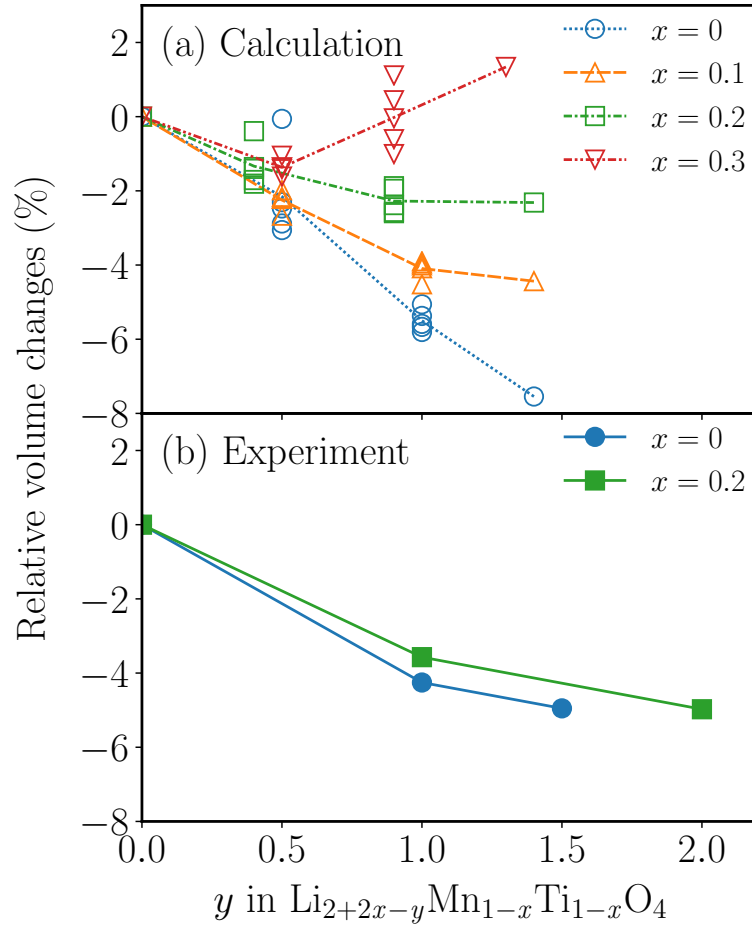
Figure 4.2: (a) Calculated relative volume changes (RVCs) with respect to $y = 0$ fully-discharged phases of the $Li_{2+2x-y}Mn_{1-x}Ti_{1-x}O_4$ as a function of y for $x =$ 0, 0.1, 0.2, and 0.3 are shown by blue spheres, orange upward triangles, green squares, and red downward triangles, respectively. Multiple same marks denote the calculated values for the different Li- and vacancy-site configurations, and mean values are connected by lines. (b) Experimental values for $x = 0$ and 0.2 are also plotted by blue dots and solid green squares, respectively.[41]

at cations around the open spaces lead to the large volume expansions. These structure charges from octahedral to tetrahedral environments for high x and y show that the rock-salt-based structure becomes unstable for high y.

Note that the calculations are performed for $Li_{2+2x-y}Mn_{1-x}Ti_{1-x}O_4$ models in whole y ranges from 0 to $2 + 2x$, but results of limited y are shown. There exists a difficulty of modeling atomic structures for high y, namely, unphysical isolated O atoms without neighboring cations appear in the models because of increasing Li vacancies with increasing y. As Li vacancy increases, most of such models show drastic crystal structure changes after the structure optimizations by the first-principles calculation, including the bond rearrangements from rock-salt-type octahedral to spine-like tetrahedral geometries and the formation of O-O bonds depending on the models. Such structure transformations lead to large volume expansions relative to the low-y models, contrary to a general expectation of decreasing RVCs with increasing y. Therefore, realistic Li-configurations in the models are preferentially selected so as not to set such isolated O atoms in the cells. However, it is inevitable to include such isolated O atoms in the models as y exceeds a certain amount y_{max}, which is referred to be the maximum number of removable Li atoms. Therefore, the calculation results of low y-region less than y_{max}, where the rock-salt-type structures are kept, are focused. The y_{max} corresponds to nearly experimentally-observed ranges.

The formation enthalpy $H_x(y)$ of the $Li_{2+2x-y}Mn_{1-x}Ti_{1-x}O_4$ as a function of y for $x = 0\text{-}0.3$ is calculated to obtain the theoretical reaction processes, shown in Fig. 4.3. $H_x(y)$ is defined as

$$H_x(y) = E_x(y) - \left(1 - \frac{y}{y_{max}}\right) E_x(0) - \frac{y}{y_{max}} E_x(y_{max}), \tag{4.24}$$

where $E_x(y)$ is the calculated total energy of $Li_{2+2x-y}Mn_{1-x}Ti_{1-x}O_4$ and y_{max} is the maximum number of removable Li amounts. The calculated $H_x(y)$ shows that the intermediate phases on the convex-hull curves between $0 \leq y \leq y_{max}$ can be thermodynamically and stably produced during the charge and discharge reaction processes. Interestingly, $H_x(y)$ of all calculated model with different Li- and vacancy-site configurations lies close to the convex-hull line, showing
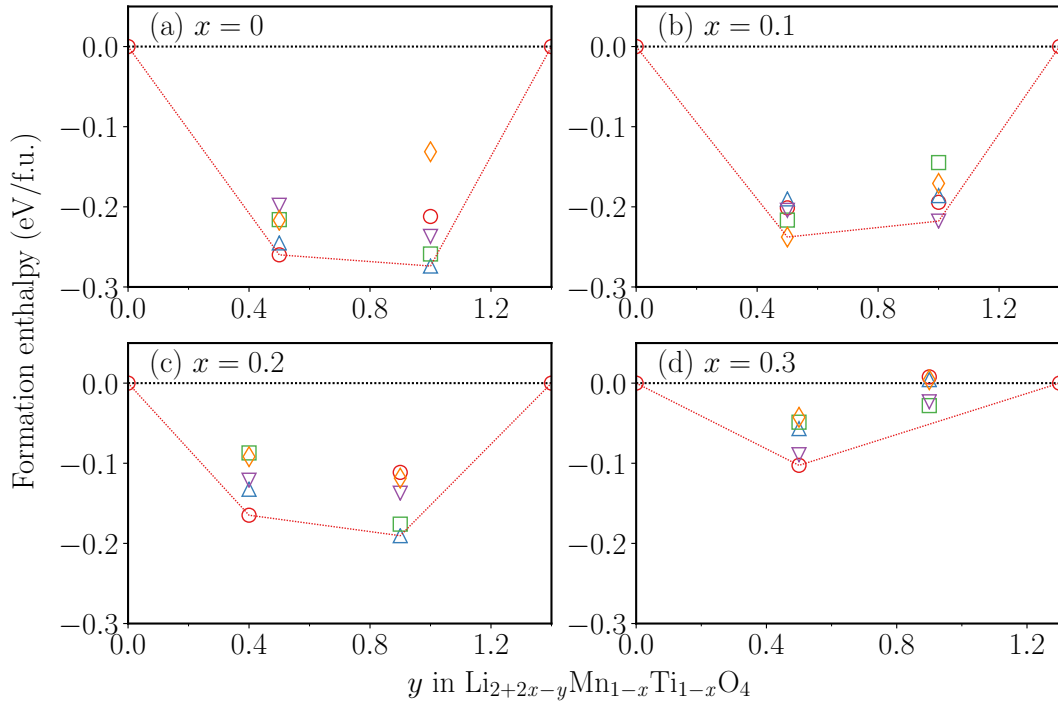
Figure 4.3: Calculated formation enthalpies of the $Li_{2+2x-y}Mn_{1-x}Ti_{1-x}O_4$ as a function of y for (a) $x = 0$, (b) 0.1, (c) 0.2, and (d) 0.3. Different marks show the calculated values for the different Li- and vacancy-site configurations, and the lowest energy values are connected with dotted red lines as convex-hull curves.

that the site configuration dependence of Li- and Li-vacancy on the structural stability is not significant. This result supports the proposed mechanism of the cation disordered structure stabilized with d^0 elements.[48] The convex-hull curve becomes shallower as x increases, showing that the structural stability of the intermediate phase decreases with increasing x. It can be speculated that the cation-disordered rock-salt structure becomes unstable for x larger than 0.3, because the element ratio of the d^0 element Ti decreases with increasing x in the cathodes.

4.3.2 Voltage-Capacity Characteristics

The voltage $V_x(y)$ is calculated by using the calculated total energy of the thermodynamically stable intermediate for a given y, shown in Fig. 4.4. The theoretical reaction proceeds along the reaction equation obtained by the calculated $H_x(y)$. Thus, $V_x(y)$ is defined as

$$V_x(y) = -\frac{E_x(y - \Delta y) - E_x(y) - \Delta y E_{Li}}{\Delta y}, \tag{4.25}$$
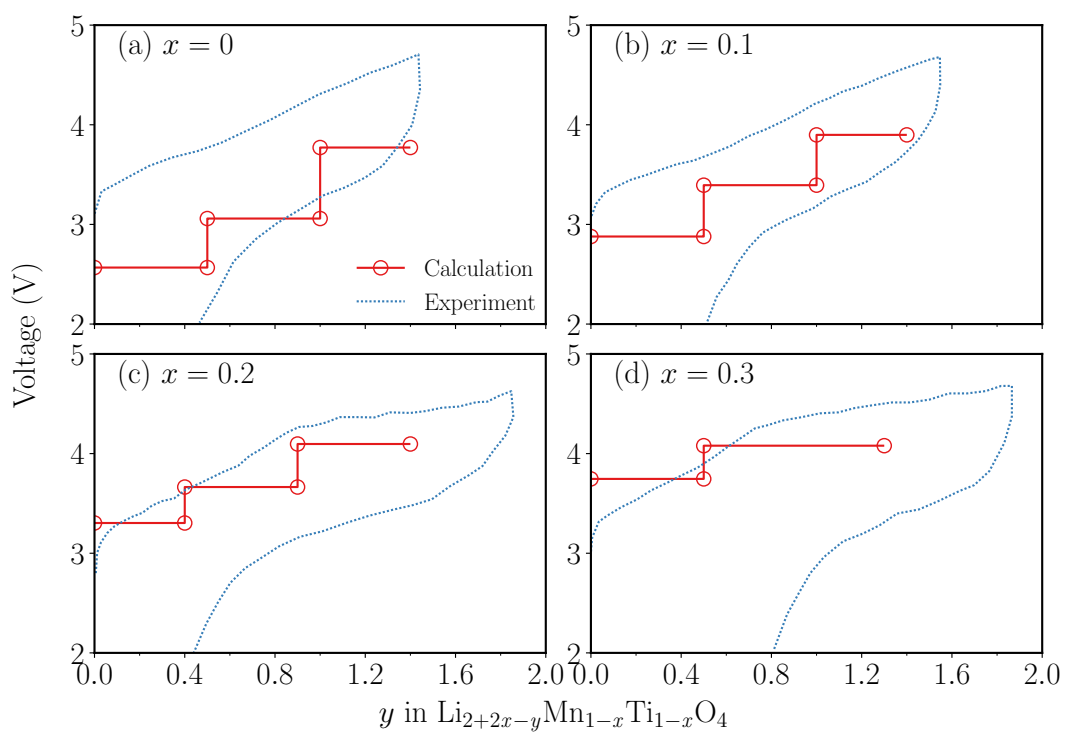
Figure 4.4: Calculated voltages of $\text{Li}_{2+2x-y}\text{Mn}_{1-x}\text{Ti}_{1-x}\text{O}_4$ as a function of y for (a) $x = 0$, (b) 0.1, (c) 0.2, and (d) 0.3 are shown by red circles with solid lines, and experimental values of the initial charge and discharge processes measured at the room temperatures are also plotted by dotted blue lines.

where Δy is transferred Li amounts and E_{Li} is the calculated total energy of a pure Li metal with BCC structure.[13] The experimental voltage-capacity curves of $\mathrm{Li}_{2+2x-y}\mathrm{Mn}_{1-x}\mathrm{Ti}_{1-x}\mathrm{O}_4$ have been reported for $x = 0$, 0.1, 0.2, and 0.3 at room temperatures,[41] and especially in charging processes for $x = 0.2$ and 0.3, show nonmonotonic behavior depending on y, *i.e.*, the voltage increases as y increases and then turn to be nearly flat. This tend possibly originates from the fact that the reaction mechanism strongly depends on y, and it was experimentally suggested that the sloping and flat voltage regions in the low and high y ranges correspond to the Mn- and O-redox reactions, which have been observed by XANES measurements.[41] The calculated $V_x(y)$ for all x increases with increasing y as the charging reactions proceed in the range of 2.57-3.77 V ($x = 0$), 2.88-3.90 V ($x = 0.1$), 3.30-4.10 V ($x = 0.2$), and 3.75-4.08 V ($x = 0.3$), and shows the slightly higher values and the narrower widths for higher x. The calculated value lies between the experimental charge and discharge voltage curves,[41] and is consistent with the previous theoretical study by Ji et al.[66]

The calculated $V_x(y)$ at low y becomes higher as x increases comparing with those at high y, though such behavior is not so clearly confirmed in the experiments. A possible reason is that nominal ionic valences of Mn in $\mathrm{Li}_{2+2x-y}\mathrm{Mn}_{1-x}\mathrm{Ti}_{1-x}\mathrm{O}_4$ should be increased with increasing Li-excess x as Mn^{2+} for $x = 0$ and Mn^{3+} for $x = 0.2$. Therefore, the Mn-redox reaction in the low-y region can differ depending on x, such as $\mathrm{Mn}^{2+}/\mathrm{Mn}^{3+}$ for $x = 0$ and $\mathrm{Mn}^{3+}/\mathrm{Mn}^{4+}$ for $x = 0.2$, leading to the higher voltage for the higher x in the lower-y region. In the high y region, where the calculated voltage is nearly unchanged and flat by x, the O-redox reaction can be dominant reaction mechanism for all x as discussed in the next section, indicative of the small voltage changes by x. The reaction mechanism is discussed in detail from analyses of electronic structures in the next section.

4.3.3 Electronic Structures and Reaction Mechanisms

The microscopic reaction mechanism in the $\mathrm{Li}_{2+2x-y}\mathrm{Mn}_{1-x}\mathrm{Ti}_{1-x}\mathrm{O}_4$ cathode is discussed on the basis of calculated electronic structure changes associated with Li-insertion and desorption. Figure 4.5 shows calculated atom-decomposed partial densities of states (PDOSs) of

$Li_{2+2x-y}Mn_{1-x}Ti_{1-x}O_4$ models for x = 0-0.5, which are site-averaged for each of elements. PDOSs of Li show that the valence states of Li for all x exist dominantly in high-energy con-
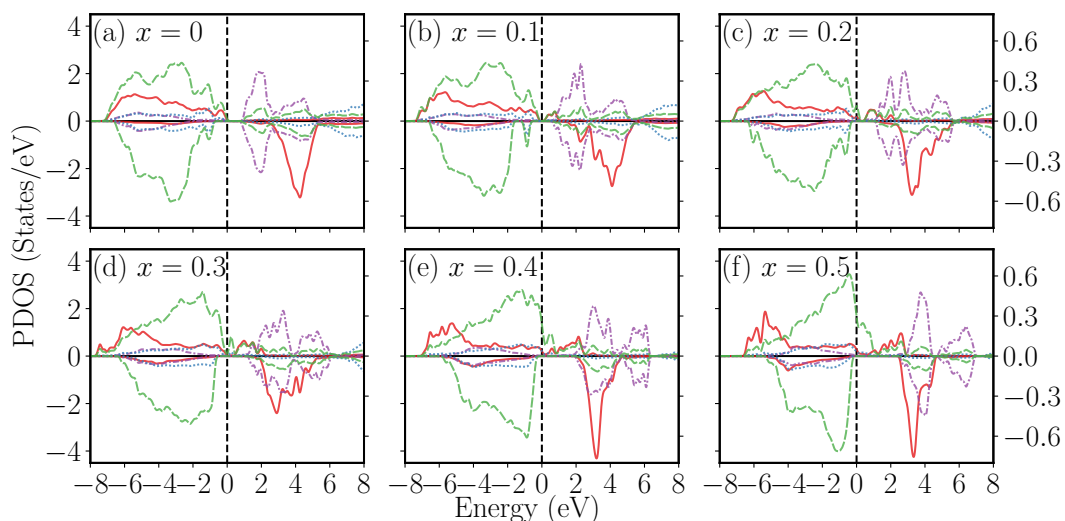
Figure 4.5: Calculated atom-decomposed partial densities of states (PDOSs) of $Li_{2+2x-y}Mn_{1-x}Ti_{1-x}O_4$ models for (a) x = 0, (b) 0.1, (c) 0.2, (d) 0.3, (e) 0.4, and (f) 0.5. PDOSs of Mn and Ti are shown by solid red lines and dash-dotted purple lines, respectively, with left scales. PDOSs of Li and O are plotted by dotted blue and dashed green lines, respectively, with right scales. The Fermi levels are shown by vertical dashed black lines.

duction band regions, indicating an ionic states of Li^+. Ti states for all x near the Fermi levels, which are dominantly d states, are almost occupied, consistent with Ti^{4+} (d^0) ionic representations, but to be precise, some Ti-d states are partially occupied due to hybridization with the O-p states. Such hybridization between the Ti-d and O-p states become smaller as x increases. The contribution of Ti-redox reaction in the Li_2MTiO_4 (M = V, Cr, Mn, Fe, Co, and Ni) with the cation-disordered rock-salt type structure was reported experimentally,[36,38] and the present result shows that such Ti-redox reaction hardly contribute to the battery reaction for high x.

PDOS of Mn for x = 0 shows the ionic nature of Mn^{2+} with $3d^5$, as the up- and down-spin states are almost occupied and unoccupied, respectively, consistent with the result in the previous part. As x increases from 0 to 0.2, the unoccupied up-spin Mn-d states increase, while the down-spin Mn-d states are kept to be almost fully unoccupied. This changes of the Mn-d states by x indicate that the valence states of Mn increase from Mn^{2+} to Mn^{3+} (d^4) by increasing x, as expected from the nominal ionic states as $Li_2^+Mn^{2+}Ti^{4+}O_4^{2-}$ (x = 0) and

$Li_{2.4}^+Mn_{0.8}^{3+}Ti_{0.8}^{4+}O_4^{2-}$ ($x = 0.2$). As x further increases larger than 0.2, the unoccupied up-spin Mn-d states further increase reaching to an ionic state of Mn^{4+} (d^3), in which the up-spin t_{2g} and e_g states in octahedral crystal fields are almost occupied and unoccupied, respectively. Such an ionic nature of Mn^{4+} can be seen for $x = 0.3$-0.5, differently from that the nominal ionic valence increases as Mn^{4+} ($x = 1/3$), Mn^{5+} ($x = 3/7$), and Mn^{6+} ($x = 0.5$) with assuming Li$^+$, Ti^{4+}, and O^{2-}. Therefore, such high oxidation states of Mn are not preferable for high x, and other elements such as O can contribute to the charge compensation instead of Mn. Actually, PDOSs of O near the Fermi levels, predominantly p characters, show that the unoccupied states increase with increasing x, contributing to the charge compensation with O for high x. The result indicates the larger contribution of the O-redox reaction to early charging processes for higher x.

Analyses of the PDOS change by y show that the Mn-redox reaction dominantly contributes to the battery reaction in the whole calculated y range for the models with $x = 0$-0.1. The valence states of Mn change as roughly Mn^{2+}, Mn^{3+}, and Mn^{4+} as y increases, and the contribution of the O-redox reaction to the charge compensation is minor, keeping O^{2-} almost independent of y. This result can account for the tend of calculated voltage-capacity curve for $x \sim 0$, which shows the continuous increments of the voltage with increasing y. As x increases to 0.2-0.3, the Mn-redox reaction predominates up to about one-electron reaction, and the PDOSs of Mn show that Mn^{3+} at $y = 0$ changes to Mn^{4+} at $y > 0$ in the cathode. In the cathodes with $x = 0.4$ -0.5, the O-redox reaction plays a major role on the battery reaction in the whole y ranges, because Mn^{4+} hardly changes to the higher valence states.

To focus on the effect of Li-insertion and desorption on electronic structures of $Li_{2+2x-y}Mn_{1-x}Ti_{1-x}O_4$, angular-momentum decomposed partial densities of states (LDOSs) are also investigated for $x = 0.2$ as a representation. Figure 4.6 shows the calculated LDOSs of $Li_{2.4-y}Mn_{0.8}Ti_{0.8}O_4$ for $y = 0$, 0.9, and 1.4, which are averaged over all sites for each element. LDOSs of Mn show that the electronic states around the Fermi levels are mainly composed of d states, and at $y = 0$, the up- and down-spin Mn-d states are roughly 4/5 filled and mostly unoccupied, respectively, corresponding to the d^4 (Mn^{3+}) electronic states. As y increases from
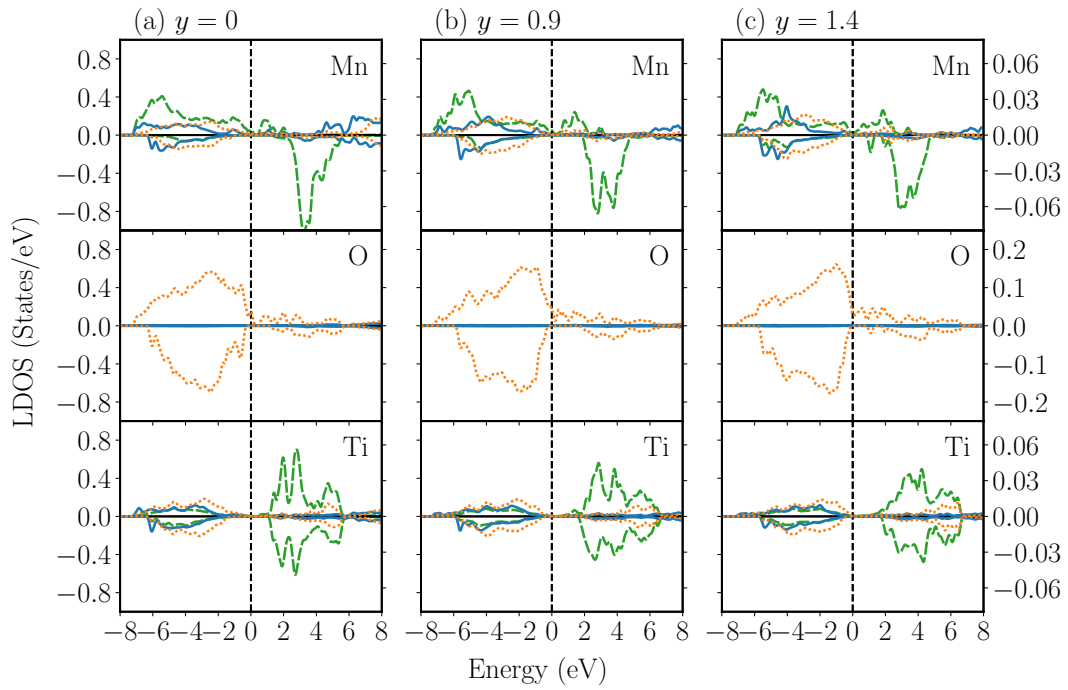
Figure 4.6: Calculated angular-momentum decomposed partial densities of states (LDOSs) projected on *s* (solid blue lines), *p* (dotted yellow lines), and *d* (dashed green lines) orbitals of Mn, O, and Ti in the $Li_{2.4-y}Mn_{0.8}Ti_{0.8}O_4$ ($x = 0.2$) models for (a) $y = 0$, (b) 0.9, and (c) 1.4. PDOSs are plotted for *s* and *p* with the right scales and for *d* with the left scales, and the Fermi levels are shown by vertical dashed black lines.

0 to 0.9, showing that the Mn valence changes from Mn^{3+} to higher oxidation states such as d^3 (Mn^{4+}). LDOSs of O show that the electronic states around the Fermi levels are predominated with the p states, and the mostly occupied p-states show an ionic character of O^{2-} at $y = 0$. The unoccupied LDOSs of O-p increase with increasing y, showing an importance of the O-redox reaction to compensate the valence changes by Li removals. LDOSs of Ti show that the d states mostly exist above the Fermi levels for all y, consistent with the d^0 (Ti^{4+}) ionic character. Based on the above findings, the calculated LDOSs show that the Mn- and O-redox reactions predominantly contribute to the battery reaction in the cathode for $x = 0.2$.

To confirm the above result on the cation- and anion-redox reactions for all x, the Bader charges relative to the $y = 0$ phases of Mn, Ti, and O for $x = 0$-0.3 are also calculated,[79–81] shown in Fig. 4.7. It can be seen that the Bader charge of Ti is practically unchanged by y for all
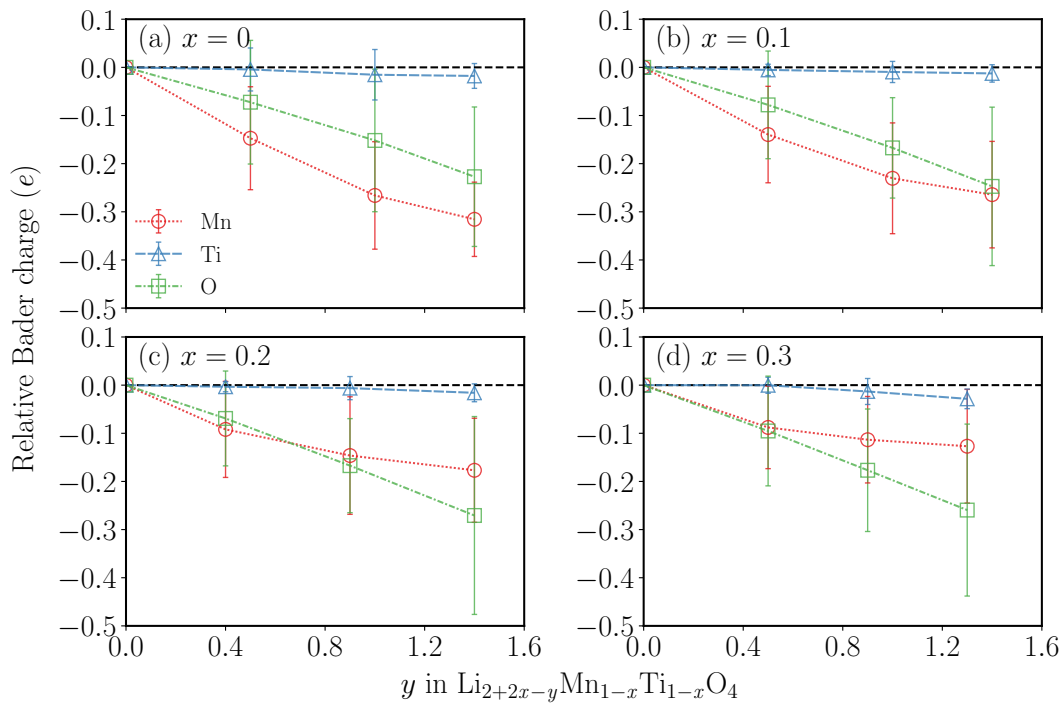
Figure 4.7: Calculated relative Badar charges with respect to the $y = 0$ phases of Mn (red circles), Ti (blue triangles), and O (green squares) in the $Li_{2+2x-y}Mn_{1-x}Ti_{1-x}O_4$ models as a function of y for (a) $x = 0$, (b) 0.1, (c) 0.2, and (d) 0.3. Mean values are connected by lines with standard deviations.

x, in contrast, that those of Mn and O strongly depend on y as well as x. For $x = 0$ and 0.1, the Bader charge of Mn decreases rapidly compared with that of O as y increases, indicating that

the dominance of Mn-redox reaction. To be precise, the slopes of the Bader charge of Mn for $x = 0$ and 0.1 become small in $y > 0.9$, and the Mn and O curves cross at $y = 1.4$ in $x = 0.1$, showing that the Mn-redox contribution is comparable to the O-redox contribution at high y. As x further increases to 0.2, 0.3, the Bader charge differences of Mn become flatter at early y regions (about $y > 0.4$), and the O-redox reaction turns to contribute largely compared with that of Mn. The calculated Bader charge analyses can confirm the predicted reaction mechanism from the electronic structure analyses.

4.3.4 Stability against O_2-Release

The O_2-release from the cathode has been pointed out for Li-excess cathode materials[82] and also for materials without Li excess ($x = 0$) as described in the previous part. The calculated PDOSs of O indicate that unoccupied O states increase as the charging reaction process proceed especially for high Li-excess x, as ionic states change from O^{2-} to the more oxidized form of O. The result possibly indicates that stability of O in the cathode becomes dropping for low Li concentration, thus a possibility of the O_2-release from the cathodes by estimating vacancy formation energies of O by comparing with those of Li.[65]

Vacancy formation energy $E_x^{V_O}(y)$ of a single neutral O vacancy V_O in the $Li_{2+2x}Mn_{1-x}Ti_{1-x}O_4$ model is defined as

$$E_x^{V_O}(y) = E_x(y, V_O) - E_x(y, 0) + \frac{E_{O_2}}{2}, \qquad (4.26)$$

where it is assumed that O is released from the cathode as the O_2-molecule with the total energy E_{O_2}, and $E_x^{V_O}(y)$ is calculated by using the 80-atom supercell models with and without V_O with the total energies $E_x(y, V_O)$ and $E_x(y, 0)$, respectively. Similarly, vacancy formation energy $E_x^{V_{Li}}(y)$ of a single neutral Li vacancy V_{Li} in $Li_{2+2x}Mn_{1-x}Ti_{1-x}O_4$ is defined as

$$E_x^{V_{Li}}(y) = E_x(y) - E_x(0) + E_{Li}, \qquad (4.27)$$

where E_{Li} is the total energy of pure Li metal, and $E_x^{V_{Li}}(y)$ is also calculated by using the super-cells with and without V_{Li} with total energies $E_x(y)$ and $E_x(0)$, respectively.

The calculated $E_x^{V_O}(y)$ and $E_x^{V_{Li}}(y)$ in $Li_{2+2x}Mn_{1-x}Ti_{1-x}O_4$ as a function of the Li-deficiency y for $x = 0$-0.3 are shown in Fig. 4.8. For all x, the dependence of V_{Li} sites on on $E_x^{V_{Li}}(y)$ is
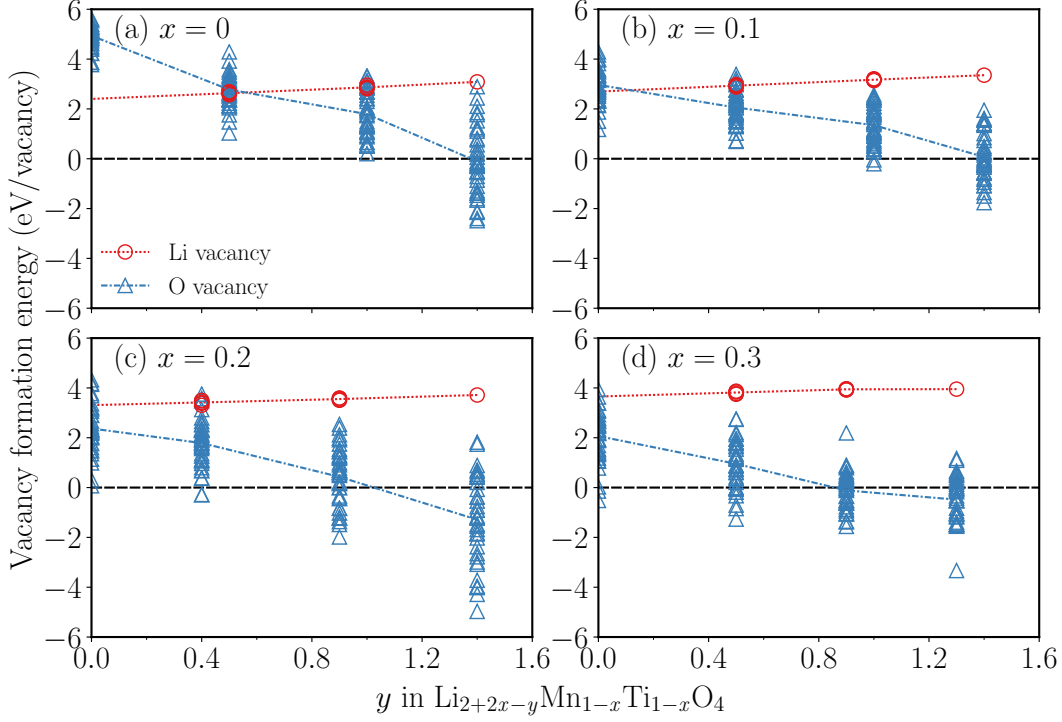
Figure 4.8: Calculated vacancy formation energies of Li and O in the $Li_{2+2x-y}Mn_{1-x}Ti_{1-x}O_4$ models as a function of the Li-deficiency y for (a) $x = 0$, (b) 0.1, (c) 0.2, and (d) 0.3 are plotted by red circles and blue triangles. Different marks denote the calculated values for different vacancy sites, and the mean values are connected by lines.

negligible small, consistent with the tend of calculated formation enthalpies in Sect. 4.3.1. And also, $E_x^{V_{Li}}(y)$ slightly increases with increasing y in a range of 3-4 eV, corresponding to relevant voltage regions. In contrast, $E_x^{V_O}(y)$ scatters in wide energy ranges and strongly depends on V_O sites, indicating that the stability of the cathodes against the O_2-release depends significantly on the geometric arrangements surrounding O to be released. $E_x^{V_O}(y)$ rapidly decreases reaching to negative values with increasing y, as reported theoretically to be the remarkable O_2-release around $y = 1.2$ for $x = 0$. The present result also shows that the O_2-release can occur easily at y larger than 1.2 for $x = 0$. The stability against the O_2-release becomes much lower as x

increases, and the O_2-release in large y ranges is not negligible to consider the battery reaction especially for $x = 0.2$ and higher. Such lower stability of O in the cathodes for high y and x explains well the experimental large irreversible capacities. Therefore, $Li_{2+2x}Mn_{1-x}Ti_{1-x}O_4$ with $x < 0.2$ is considered to be a better candidate material in terms of the structural stability against the O_2-release, and the O_2-release at low Li concentration for high Li-excess x in the cathodes obstructs improvements of the battery performances.

4.3.5 Effects of Li-Excess x on the Battery Reaction

The microscopic reaction mechanism including the O_2-release in the $Li_{2+2x}Mn_{1-x}Ti_{1-x}O_4$ cathode is systematically discussed on the basis of calculated electronic structures and vacancy formation energies of Li and O. Figure 4.9 shows that the upper limits and lower limits of calculated voltages and the y_c values for the O_2-release, in which calculated vacancy formation energies of O have negative values. The lower limit of the calculated voltage increases with
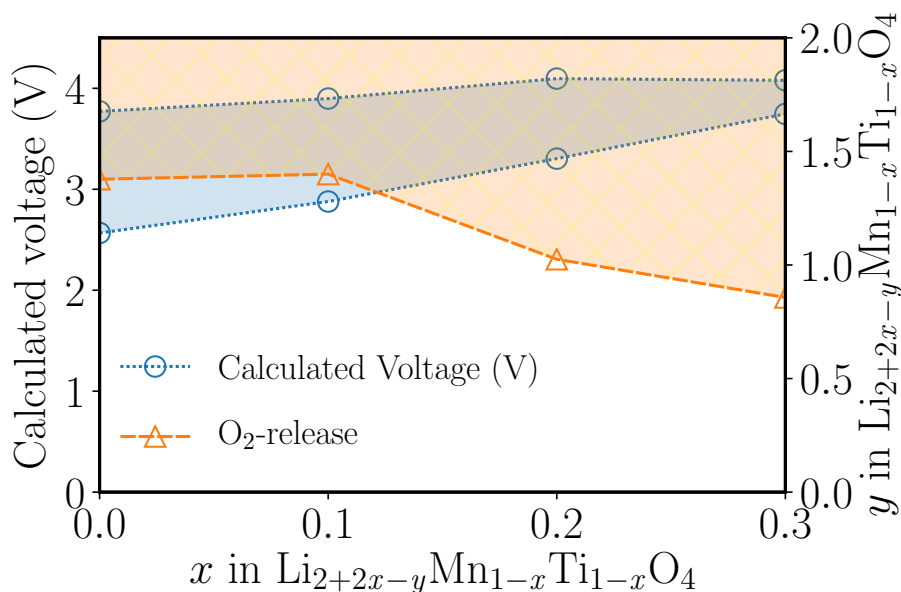
Figure 4.9: Upper limits and lower limits of the calculated voltages for $Li_{2+2x-y}Mn_{1-x}Ti_{1-x}O_4$ are shown by blue circles with dotted lines. Evaluated critical Li deficiency y_c in $Li_{2+2x-y}Mn_{1-x}Ti_{1-x}O_4$ are shown by orange triangles with a dashed line. The calculated vacancy formation energies of O have negative values in the orange hatched area, which are in the y range higher than y_c.

increasing x, but the upper limit of them is almost same for $x = 0.2$ and 0.3, indicating that the

O-redox reaction primarily contributes to the charge compensation on the Li removal. The O_2-release is more appreciable for higher x region than $x = 0.2$. Therefore, $Li_{2+2x}Mn_{1-x}Ti_{1-x}O_4$ with $x < 0.2$ is considered to be good candidate material for the commercial use.

4.4   Conclusion

The effect of the Li-excess x (x = 0-0.3) as well as the number of removable Li amounts y in $Li_{2+2x-y}Mn_{1-x}Ti_{1-x}O_4$ on the cathode properties of the volume changes, voltage-capacity characteristics, electronic structures, and structural stability against the O_2-release were theoretically studied using the first-principles calculation. The cathode reaction mechanism associated with cation- and anion-redox reactions depend on x and y significantly, changing from the Mn-redox reaction to the O-redox reaction with increasing y. The O-redox reaction has much remarkable effects at high y for high x in the cathode, and also the O_2-release from the cathode can occur easier for high x at high y. Therefore, the materials with $x < 0.2$ are considered to be good x in terms of the stability of O.

Part IV

Conclusion

In order to establish the sustainable society, large-scale battery systems are strongly required, and the Li-ion battery has attracted much interest because it has higher voltage, higher capacity, and higher energy density among the rechargeable batteries. Important battery characteristics such as the voltage, capacity, and energy density are predominantly determined by the cathode material, thus many researchers have experimentally and theoretically investigated the cathode materials with the good battery performances, reporting that transition-metal oxides with well-ordered structures show the high battery performances. $LiCoO_2$ with the layered-rock-salt-type structure, $LiFePO_4$ with the olivine-type structure, and $LiMn_2O_4$ with the spinel-type structure are commercially success as the cathode materials. However, to implement the Li-ion batteries for the future electric vehicles and renewable energy power plants, the cathode materials with exceeding capacities of previous systems are required. Furthermore, paying much attentions to materials costs, safety, and environmental impacts are also desired. The oxides of the cation-disordered rock-salt type are expected to be alternative cathode materials to replace the conventional oxides of the well ordered type because of their high structural stability at low Li concentration and enormous degrees of freedom in the chemical composition.

In this thesis, to clarify effects of cation-element compositions and Li-excess amounts on the battery performances in the oxides of the cation-disordered rock-salt type, Li_2MTiO_4 (M = V, Cr, Mn, Fe, Co, and Ni) and Li-excess phases, $Li_{2+2x}Mn_{1-x}Ti_{1-x}O_4$ ($0 \leq x \leq 0.3$), were systematically investigated by using the first-principles calculations.

In the first part of this thesis, the effect of cation-element compositions on the battery performance in Li_2MTiO_4 (M = V, Cr, Mn, Fe, Co, and Ni) was focused, and the systematic understandings for transition-metal series were firstly given. The structural stability and voltage-capacity characteristics were theoretically investigated and compared to the experimental result, and the microscopic reaction mechanism including the O_2-release from the cathode was also discussed on the basis of the calculated electronic structures and vacancy formation energies of Li and O. The microscopic reaction mechanism of Li_2MTiO_4 (M = V, Cr, Mn, Fe, Co, and Ni) is mainly associated with the M- and O-redox reactions in addition to the minor Ti-redox reaction at high and low Li concentrations in the cathode. As M changes from V to

Ni, the O-redox reaction shows a significantly role on the charge compensation especially at low Li concentration, originating from the fact that M-$3d$ and O-$2p$ states shift to lower and higher energy levels, respectively, with respect to the Fermi level with increasing number of $3d$ electrons in M. The O-$2p$ states have high peaks around the Fermi levels at low Li concentration for the large number of $3d$ electrons in M, and make electronic structures unstable, inducing the easier O_2-release from the cathode contrary to the expectation. The high voltage and high structural stability against the O_2-release are trade-off relation, thus it was proposed that Li_2CrTiO_4 cathode may be the best candidate cathode material among the present calculation.

In the second part of this thesis, the effect of Li-excess amounts on the battery performance in $Li_{2+2x}Mn_{1-x}Ti_{1-x}O_4$ ($0 \leq x \leq 0.3$) was focused, and uppers limit of the Li-excess amount in these cathodes were discussed. The changes of the structural stability with increasing x were theoretically investigated, indicating that the structural stability lowers for larger x than 0.2 originating from decreasing ratio of d^0 element Ti. Although stoichiometric oxidation states of Mn change from Mn^{2+} ($x = 0$) to Mn^{6+} ($x = 0.5$), the calculated electronic structures show that Mn does not change from Mn^{4+} to the more oxidized states as x increases. Instead of Mn, O plays a significant role in the charge compensation on Li removals. The Mn- and O-redox reactions predominantly and supplementary contribute to the battery reaction at high and low Li concentrations for lower x than 0.2, but the contribution of the O-redox reaction for larger x than 0.2 are appreciable compared with those of Mn. The voltage-capacity profiles show the flat behavior and narrower width of the potential window in the region of the O-redox reaction. The O-redox reaction induces high peaks around the Fermi levels in the DOSs. The calculated vacancy formation energies of Li and O indicate that the O_2-release from the cathode become much remarkable at lower Li concentration in larger x. An enhancement of the rechargeable capacities by increasing Li-excess amounts in $Li_{2+2x}Mn_{1-x}Ti_{1-x}O_4$ can be obstructed by the O_2-release from the cathodes, and the cathodes for $x < 0.2$ are considered to be good x in terms of the structural stability against the O_2-release.

Several cathode materials have been proposed since 1991, but existing cathode materials are not fully replaced. The oxides of the cation-disordered rock-salt type reported as cathode

materials recently have high potential to be the future positive electrode, and further studies are required both experimentally and theoretically. I believe that the studies in this thesis give valuable information about the theoretical research schemes, and helpful to improve the battery performances in the aspect of transition-metal compositions and Li-excess amounts.

Bibliography

[1] M. S. Whittingham, F. R. Gamble Jr, Mater. Res. Bull. 10 (1975) 363.

[2] N. Nitta, F. Wu, J. T. Lee, G. Yushin, Mater. Today 18 (2015) 252.

[3] K. Mizushima, P. C. Jones, P. J. Wiseman, J. B. Goodenough, Mater. Res. Bull. 15 (1980) 783.

[4] A. Yoshino, K. Sanechika, T. Nakajima, Japanese patent no. 1989293, (1985)

[5] Editor:D. Linden, T. B. Reddy, HANDBOOK OF BATTERIES-Third Edition, McGraw-Hill (2001)

[6] K. Momma, F. Izumi, J. Appl. Crystallogr. 44 (2011) 1272.

[7] D. C. Harris, Quantitative Chemical Analysis-Seventh Edition, W. H. Freeman and Company (2007)

[8] A. Urban, D.-H. Seo, G. Ceder, NPJ Comput. Materi. 2 (2016) 16002.

[9] S. P. Ong, V. L. Chevrier, G. Hautier, A. Jain, C. Moore, S. Kim, X. Ma, G. Ceder, Energy Environ. Sci. 4 (2011) 3680.

[10] J.-M. Tarascon, M. Armand, Nature 414 (2001) 359.

[11] M. M. Thackeray, P. J. Johnson, L. A. de Picciotto P. G. Bruce, and J. B. Goodenough, Mater. Res. Bull. 19 (1984) 179.

[12] A. K. Padhi, K. S. Nanjundaswamy, and J. B. Goodenough, J. Electrochem. Soc. 144 (1997) 1188.

[13] M. K. Aydinol, A. F. Kohan, G. Ceder, K. Cho, J. Joannopoulos, Phys. Rev. B 56 (1997) 1354.

[14] M. K. Aydinol, G. Ceder, J. Electrochem. Soc. 144 (1997) 3832.

[15] P. Tang, N. A. W. Holzwarth, Phys. Rev. B 68 (2003) 165107.

[16] W. Li, J. C. Currie, J. Wolstenholme, J. Power Sources 68 (1997) 565.

[17] G. Dutta, A. Manthiram, J. B. Goodenough, J. C. Grenier, J. Solid State Chem. 96 (1992) 123.

[18] A. Hirano, R. Kanno, Y. Kawamoto, Y. Takeda, K. Yamamura, M. Takano, K. Ohyama, M. Ohashi, Y. Yamaguchi, Solid State Ionics 78 (1995) 123.

[19] D. D. MacNeil, Z. Lu, J. R. Dahn, J. Electrochem. Soc. 149 (2002) A1332.

[20] Y. Idemoto, T. Matsui, Electrochemistry 75 (2007) 791.

[21] P. Hohenberg, W. Kohn, Phys. Rev. 136 (1964) B864.

[22] A. R. Oganov, C. W. Glass, J. Chem. Phys. 124 (2006) 244704.

[23] A. R. Oganov, A. O. Lyakhov, M. Valle, Acc. Chem. Res. 44 (2011) 227.

[24] A. O. Lyakhov, A. R. Oganov, H. T. Stokes, Q. Zhu, Comp. Phys. Comm. 184 (2013) 1172.

[25] T. Yamashita, N. Sato, H. Kino, T. Miyake, K. Tsuda, T. Oguchi, Phys. Rev. Mater. 2 (2018) 013803.

[26] K. Terayama, T. Yamashita, T. Oguchi, K. Tsuda, NPJ Comput. Materi. 4 (2018) 32.

[27] T. Yamashita, H. Momida, and T. Oguchi, Electrochim. Acta 195 (2016) 1.

[28] H. Kotaka, H. Momida, A. Kitajou, S. Okada, T. Oguchi, Chem. Rec. 19 (2019) 811.

[29] H. Kotaka, H. Momida, A. Kitajou, S. Okada, T. Oguchi, J. Comput. Chem. Jpn. 18 (2019) 78.

[30] H. Momida, A. Kitajou, S. Okada, T. Yamashita, T. Oguchi, J. Phys. Soc. Jpn. 84 (2015) 124709.

[31] L. Sebastian, J. Gopalakrishnan, J. Solid State Chemistry 172 (2003) 171.

[32] S. R. S. Prabaharan, M. S. Michael, H. Ikuta, Y. Uchimoto, M. Wakihara, Solid State Ionics 172 (2004) 39.

[33] M. Küzma, R. Dominko, A. Meden, D. Makovec, M. Bele, J. Jamnik, M. Gaberšček, J. Power Sources 189 (2009) 81.

[34] M. Kuezma, R. Dominko, D. Hanžel, A. Kodre, I. Arčon, A. Meden, M. Gaberšček, J. Electrochem. Soc. 156 (2009) A809.

[35] R. Dominko, C. V.-A. Garrido, M. Bele, M. Kuezma, I. Arcon, M. Gaberscek, J. Power Sources 196 (2011) 6856.

[36] M. Yang, X. Zhao, Y. Bian, L. Ma, Y. Ding, X. Shen, J. Mater. Chem. 22 (2012) 6200.

[37] R. Trócoli, M. Cruz-Yusta, J. Morales, J. Santos-Peña, Electrochimica Acta 100 (2013) 93.

[38] Y. Kawano, A. Kitajou, S. Okada, J. Power Sources 242 (2013) 768.

[39] Y. Wang, Y. Wang, F. Wang, Nanoscale Res. Lett. 9 (2014) 197.

[40] X. Zhang, L. Yang, F. Hao, H. Chen, M. Yang, D. Fang, Nanomaterials 5 (2015) 1985.

[41] A. Kitajou, K. Tanaka, H. Miki, H. Koga, T. Okajima, S. Okada, Electrochemistry 84 (2016) 597.

[42] J. Lee, A. Urban, X. Li, D. Su, G. Hautier, G. Ceder, Science 343 (2014) 519.

[43] J. Lee, D.-H. Seo, M. Balasubramanian, N. Twu, X. Li, G. Ceder, Energy Environ. Sci. 8 (2015) 3255.

[44] J. Lee, J. K. Papp, R. J. Clément, S. Sallis, D.-H. Kwon, T. Shi, W. Yang, B. D. McCloskey, G. Ceder, Nat. Commun. 8 (2017) 981.

[45] M. Okubo, A. Yamada, ACS Appl. Mater. Interfaces 9 (2017) 36463.

[46] N. Yabuuchi, M. Nakayama, M. Takeuchi, S. Komaba, Y. Hashimoto, T. Mukai, H. Shiiba, K. Sato, Y. Kobayashi, A. Nakao, M. Yonemura, K. Yamanaka, K. Mitsuhara, T. Ohta, Nat. Commun. 7 (2016) 13814.

[47] N. Yabuuchi, Chem. Lett. 46 (2017) 412.

[48] A. Urban, A. Abdellahi, S. Dacek, N. Artrith, G. Ceder, Phys. Rev. Lett. 119 (2017) 176402.

[49] J. F. Janak, V. L. Moruzzi, A. R. Williams, Phys. Rev. B 12, (1975) 1257.

[50] M. Weinert, J. Math. Phys. 22 (1981) 2433.

[51] W. Wimmer, H. Krakauer, M. Weinert, A. J. Freeman, Phys. Rev. B 24 (1981) 864.

[52] J. M. Soler, A. R. Williams, Phys. Rev. B 40 (1989) 1560.

[53] J. M. Soler, A. R. Williams, Phys. Rev. B 42 (1990) 9728.

[54] D. D. Koelling, B. N. Harmon, J. Phys. C 10 (1977) 3107.

[55] First-principles calculation code package HiLAPW (http://www.cmp.sanken.osaka-u.ac.jp/˜oguchi/HiLAPW/index.html).

[56] T. Oguchi, H. Momida, J. Phys. Soc. Jpn. 82 (2013) 065004.

[57] H. Momida, T. Yamashita, T. Oguchi, J. Phys. Soc. Jpn. 83 (2014) 124713.

[58] T. Yamashita, H. Momida, T. Oguchi, J. Phys. Soc. Jpn. 84 (2015) 074703.

[59] A. Kitajou, H. Momida, T. Yamashita, T. Oguchi, S. Okada ACS Appl. Energy Mater. 2 (2019) 5968.

[60] H. Momida, A. Kitajou, S. Okada, T. Oguchi, J. Phys. Soc. Jpn. 88 (2019) 124709.

[61] P. E. Blöchl, O. Jepsen, O. K. Andersen, Phys. Rev. B 49 (1994) 16223.

[62] F. D. Murnaghan, Proc. Nat. Acad. Sci. U.S.A. 30 (1944) 244.

[63] M. Nishijima, T. Ootani, Y. Kamimura, T. Sueki, S. Esaki, S. Murai, K. Fujita, K. Tanaka, K. Ohira, Y. Koyama, I. Tanaka, Nat. Commun. 5 (2014) 4553.

[64] C. Wang, J. Hong, Electrochem. Solid-State Lett. 10 (2007) A65.

[65] C. G. Van de Walle, J. Neugebauer, J. Appl. Phys. 95 (2004) 3851.

[66] H. Ji, A. Urban, D. A. Kitchaev, D.-H. Kwon, N. Artrith, C. Ophus, W. Huang, Z. Cai, T. Shi, J. C. Kim, H. Kim, G. Ceder, Nat. Commun. 10 (2019) 592.

[67] B. Huang, R. Wang, Y. Gong, B. He, H. Wang, Front. Chem. 7 (2019) 107.

[68] A. Zunger, S.-H. Wei, L. G. Ferreira, J. E. Bernard, Phys. Rev. Lett. 65 (1990) 353.

[69] A. van de Walle, M. Asta, G. Ceder, CALPHAD 26 (2002) 539.

[70] A. van de Walle, P. Tiwary, M. de Jong, D. L. Olmsted, M. Asta, A. Dick, D. Shin, Y. Wang, L.-Q. Chen, Z.-K. Liu, CALPHAD 42 (2013) 13.

[71] K. Okhotnikov, T. Charpentier, S. Cadars, ChemInform. 8 (2016) 17.

[72] J. P. Perdew, K. Burke, M. Ernzerhof, Phys. Rev. Lett. 77 (1996) 3865. [Errata 78 (1997) 1396].

[73] M. Cococcioni, S. de Gironcoli, Phys. Rev. B 71 (2005) 035105.

[74] G. Hautier, S. P. Ong, A. Jain, C. J. Moore, G. Ceder, Phys. Rev. B 85 (2012) 155208.

[75] P. Giannozzi, S. Baroni, N. Bonini, M. Calandra, R. Car, C. Cavazzoni, D. Ceresoli, G. L. Chiarotti, M. Cococcioni, I. Dabo, A. D. Corso, S. de Gironcoli, S. Fabris, G. Fratesi, R. Gebauer, U. Gerstmann, C. Gougoussis, A. Kokalj, M. Lazzeri, L. Martn-Samos, N. Marzari, F. Mauri, R. Mazzarello, S. Paolini, A. Pasquarello, L. Paulatto, C. Sbraccia, S. Scandolo, G. Sclauzero, A. P. Seitsonen, A. Smogunov, P. Umari, R. M. Wentzcovitch, J. Phys. : Condens. Matter 21 (2009) 395502.

[76] P. Giannozzi, O. Andreussi, T. Brumme, O. Bunau, M. B. Nardelli, M. Calandra, R. Car, C. Cavazzoni, D. Ceresoli, M. Cococcioni, N. Colonna, I. Carnimeo, A. D. Corso, S. de Gironcoli, P. Delugas, R. A. DiStasio Jr, A. Ferretti, A. Floris, G. Fratesi, G. Fugallo, R. Gebauer, U. Gerstmann, F. Giustino, T. Gorni, J. Jia, M. Kawamura, H.-Y. Ko, A. Kokalj, E. Kükçükbenli, M. Lazzeri, M. Marsili, N. Marzari, F. Mauri, N. L. Nguyen, H.-V. Nguyen, A. Otero-de-la-Roza, L. Paulatto, S. Poncé, D. Rocca, R. Sabatini, B. Santra, M. Schlipf, A. P. Seitsonen, A. Smogunov, I. Timrov, T. Thonhauser, P. Umari, N. Vast, X. Wu, S Baroni, J. Phys. : Condens. Matter 29 (2017) 465901.

[77] P. E. Blöchl, Phys. Rev. B 50 (1994) 17953.

[78] A. Dal Corso, Comput. Mater. Sci. 95 (2014) 337.

[79] W. Tang, E. Sanville, G. Henkelman, J. Phys.: Condens. Matter. 21 (2009) 084204.

[80] E. Sanville, S. D. Kenny, R. Smith, G. Henkelman, J. Comp. Chem. 28 (2007) 899.

[81] G. Henkelman, A. Arnaldsson, H. Jónsson, Comput. Mater. Sci. 36 (2006) 354.

[82] K. Luo, M. R. Roberts, R. Hao, N. Guerrini, D. M. Pickup, Y.-S. Liu, K. Edström, J. Guo, A. V. Chadwick, L. C. Duda, P. G. Bruce, Nat. Chem. 8 (2016) 684.

List of Achievements

Publications

1. <u>Motoyuki Hamaguchi</u>, Hiroyoshi Momida, Tamio Oguchi, "First-Principles Study on Cathode Properties of $Li_2M TiO_4$ (M = V, Cr, Mn, Fe, Co, and Ni) with Oxygen Deficiency for Li-Ion Batteries", J. Phys. Soc. Jpn. 87 (2018) 044805.

2. <u>Motoyuki Hamaguchi</u>, Hiroyoshi Momida, Tamio Oguchi, "Significant role of oxygen redox reaction with O_2-release in Li-excess cation-disordered rock-salt cathodes $Li_{2+2x}Mn_{1-x}Ti_{1-x}O_4$: First-principles calculations", Electrochimica Acta 330 (2020) 135285.

3. <u>Motoyuki Hamaguchi</u>, Hiroyoshi Momida, Tamio Oguchi, "Electronic Structure Analyses of Cation-Disordered Rock-Salt Type Cathode Materials for the Li-Ion Battery by First-Principles Calculations", Case Studies of Analyses, Examinations, and Evaluation Techniques for the Li-Ion Battery: Chapter 1-Section 3, Technical Information Institute Co., LTD. (2019) in Japanese.

International Conferences

1. <u>Motoyuki Hamaguchi</u>, Hiroyoshi Momida, and Tamio Oguchi, "First-Principles Study of Cation Disordered Rock Salt Type Oxides for Lithium Ion Battery Cathode", The 19th Asian Workshop on First-Principles Electronic Structure Calculations, (2016) Poster: 03.

2. <u>Motoyuki Hamaguchi</u>, Hiroyoshi Momida, and Tamio Oguchi, "First-Principles Study on Cathode Properties of Li-excess Rock-Salt Type $Li_{2+2x}Mn_{1-x}Ti_{1-x}O_4$", The 19th International Meeting on Lithium Batteries, (2018) P-363.

3. <u>Motoyuki Hamaguchi</u>, Hiroyoshi Momida, and Tamio Oguchi, "O_2-release and Structure Evolution of Layered $Li_{1.2}M_{0.4}M'_{0.4}O_2$ (M, M' = Cr, Mn, Ti) Cathodes for Li-Ion

Batteries: First-Principles Calculations", The 22nd Asian Workshop on First-Principles Electronic Structure Calculations, (2019) P-32.

4. <u>Motoyuki Hamaguchi</u>, Hiroyoshi Momida, and Tamio Oguchi, "First-Principles Study on Cation-Disordered Rock-Salt Type Cathode $Li_{2.4}M1_{0.8}M2_{0.8}O_4$ ($M1$, $M2$ = Ti, Cr, and Mn) for Li-Ion Batteries", Materials Research Meeting 2019, (2019) F1-13-P39.

Domestic Conferences

1. <u>Motoyuki Hamaguchi</u>, Hiroyoshi Momida, and Tamio Oguchi, "Analysis of the electronic structure of the cation disordered rock salt-type cathode compounds for lithium ion battery using the first-principles calculations." The 71st Annual Autumn Meeting of the Physical Society of Japan, (2016) 14pPSA-16.

2. <u>Motoyuki Hamaguchi</u>, Hiroyoshi Momida, and Tamio Oguchi, "First-Principles Study of Electronic Structures of Oxygen Vacancies in Cation-Disordered Rock-Salt Type Cathode Li_2MTiO_4 (M = V, Mn, Fe, Co, and Ni)", The 72nd Annul Spring Meeting of the Physical Society of Japan, (2017) 18aC-PS-28.

3. Yuuki Kawamura, Ayuko Kitajou, <u>Motoyuki Hamaguchi</u>, Hiroyoshi Momida, Tamio Oguchi, and Shigeto Okada, "Characteristics and thermodynamical Stability of Li-Excess Cation-Disordered Rock-Salt Type Cathodes for Li-Ion Rechargeable Battery", The 84th Annual Meeting of the Electrochemical Society of Japan (2017) PBT06. in Japanese.

4. <u>Motoyuki Hamaguchi</u>, Hiroyoshi Momida, and Tamio Oguchi "First-Principles Study of Electronic Structures of Li-excess Rock-Salt Type Cathode $Li_{2+2x}Mn_{1-x}Ti_{1-x}O_4$" The 73rd Annul Autumn Meeting of the Physical Society of Japan (2017) 23pPSA-87.

5. <u>Motoyuki Hamaguchi</u>, Hiroyoshi Momida, and Tamio Oguchi, "Reaction Analyses of Li-excess Rock-Salt Type Cathode $Li_{2+2x}Mn_{1-x}Ti_{1-x}O_4$ using First-Principles Calculations", The 85th Annual Meeting of the Electrochemical Society of Japan (2018) PS-52.

6. <u>Motoyuki Hamaguchi</u>, Hiroyoshi Momida, and Tamio Oguchi, "First-Principles Study on Electronic Structures in Cation-Disordered Rock-Salt Type Cathode $Li_{2+2x}Mn_{1-x}Ti_{1-x}O_4$", The 59th Battery Symposium in Japan (2018) 2C09.

7. Ayuko Kitajou, <u>Motoyuki Hamaguchi</u>, Liwei Zhao, Hiroyoshi Momida, Tamio Oguchi, Koji Abe, and Shigeto Okada, "Thermal stability of oxygen redox-type cathode for Li-ion batteries", The 59th Battery Symposium in Japan (2018) 3C13.

8. <u>Motoyuki Hamaguchi</u>, Hiroyoshi Momida, and Tamio Oguchi, "First-Principles Study on X-ray Absorption Spectroscopy of Li-excess Cation-Disordered Rock-Salt Type $Li_{2.4}Mn_{0.8}Ti_{0.8}O_4$ Cathode", The Annual Meeting of the Electrochemical Society of Japan (2019) 1I06.

9. Ayuko Kitajou, Yu Mizukami, <u>Motoyuki Hamaguchi</u>, Hiroyoshi Momida, Nobuko Yoshimoto, Tamio Oguchi and Shigeto Okada, "Cathode Properties of Layered/disordered Rocksalt-type $Li_{2.4}Cr_{0.8}M_{0.8}O_4$ (M = Mn, Ti)", The 87th Annual Meeting of the Electrochemical Society of Japan (2020) 1I17.: Accepted.

10. <u>Motoyuki Hamaguchi</u>, Hiroyoshi Momida, Ayuko Kitajou, Shigeto Okada, and Tamio Oguchi, "Electronic Structure Analyses of Li-Excess Cation-Disordered Rock-Salt Type Cathode $Li_{2.4}M_{0.8}M'_{0.8}O_4$ (M, M' = Cr, Mn, Ti): First-Principles Calculations", The 87th Annual Meeting of the Electrochemical Society of Japan (2020) 1I18.: Accepted.